Summer 12-16-2023

Environmental Fate of Sulfur in Sulphur Creek, Valles Caldera, NM: Implications for Metal Transport and Water Quality

Daniel Lavery
University of New Mexico - Main Campus

Daniel Lavery

Candidate

Earth and Planetary Science

Department

This thesis is approved, and it is acceptable in quality and form for publication:

Approved by the Thesis Committee:

Dr. Laura Crossey , Chairperson

Dr. Tobias Fischer

Dr. Ricardo González-Pinzón

Dr. Karl Karlstrom

Environmental Fate of Sulfur in Sulphur Creek, Valles Caldera, NM: Implications for Metal Transport and Water Quality

By

Daniel Joseph Lavery

B.S., Geosciences, Texas Tech University, 2021

Thesis

Submitted in Partial Fulfillment of the Requirements for the Degree of

Master of Science

Earth and Planetary Sciences

The University of New Mexico

Albuquerque, NM

December 2023

Acknowledgements

I thank my graduate committee (Laura Crossey, Tobias Fischer, Ricardo González-Pinzón, and Karl Karlstrom) for their expertise in contributing to this research. Laura Crossey has been a constant source of knowledge and motivation to find fresh perspectives on the scientific problems found in this project. I would like to thank Brionna O'Connor and Kambray Townsend for their assistance with field and lab work in the course of this project. Zach Strasberg has spent many hours helping me think of new ways to visualize and discuss my data. Drs. Mehdi Ali, Laura Burkemper, and Victor Polyak provided exceptional help in lab analyses in the Analytical Chemistry, Stable Isotope, and Radiogenic Isotope Laboratories. Dr. Robert Parmenter and Dave Pittenger of the Valles Caldera National Preserve were always quick to respond to requests for site conditions and data. I also thank my parents, Kevin and Katie Lavery for their many years investing their time and money into ensuring that I received a quality education (and for gently reminding me to value that education and the effort they put into it). I also thank you for teaching me to enjoy learning, reading, hiking, and growing.

Financial support for this project was provided by the New Mexico Water Resources Research Institute (Student Water Research Grant Q02369), the New Mexico Geological Society (Graduate Grants-In-Aid), and Geological Society of America (Graduate Grants-In-Aid) and the Department of Earth and Planetary Science (Trauger Graduate Scholarship).

Environmental Fate of Sulfur in Sulphur Creek, Valles Caldera, NM: Implications for Metal Transport and Water Quality

By

Daniel Joseph Lavery

B.S., Geosciences, Texas Tech University, 2021

M.S., Earth and Planetary Sciences, The University of New Mexico, 2023

Abstract

The 1.2 Ma Valles Caldera in north-central New Mexico hosts a young igneous volcanic hydrothermal system after the model proposed in Goff and Janik (2000). The Sulphur Springs area within Valles Caldera is an acid-sulfate area typical of this model, discharging acidic waters (pH 1.5-3) formed by oxidation of magmatic H_2S at the surface. We report on samples obtained from springs and streams collected between October 2021 and May 2023 in the Sulphur Creek and Alamo watersheds. Sulphur Creek receives input from Sulphur Springs and exhibits low pH (2-4) and high concentrations of Al (≤110 mg/L), Fe (≤60 mg/L) and sulfate (≤1300 mg/L). These hydrothermal components are significantly attenuated by the downstream extent of the field area. This investigation uses geochemical tracers such as major ions, stable and radiogenic isotopes to identify processes controlling attenuation. This research has significance for the continued use of geothermally-affected watersheds as water resources.

Contents

List of Figures

List of Tables

1. Introduction

Volcanic hydrothermal systems discharge thermal waters that can negatively impact water quality of the surface hydrologic system (Nordstrom et al., 2009; McCleskey et al., 2010a; McCleskey et al., 2010b; Golla, 2019). Hydrothermal systems such as those associated with the Valles Caldera and Yellowstone in Wyoming have been studied by Goff and Janik (2000). Goff and others (1988) investigated the hydrothermal plume originating from the Valles Caldera and concluded that the thermal springs along the Jemez Fault Zone (Soda Dam and Jemez Springs) originate from this plume. McGibbon and others (2018) extend the reach of the Valles plume down to the Tierra Amarilla warm carbonic springs near San Ysidro, NM. Golla (2019) studied the impacts of thermal springs on the natural salinization of a large stretch (~50 km) of the Jemez River (Figure 1). McCleskey and others (2010a, 2010b) investigated natural attenuation of Yellowstone hydrothermal components in the Gibbon River. The research presented in this thesis builds on the previous work done on the Valles and Yellowstone hydrothermal systems and their effects on surface water quality. **The purpose of this research is to determine geochemical and hydrologic factors that control water quality in geothermally affected watersheds. This research also functions to add detail to our understanding of the geochemistry of the Valles acid-sulfate features. We hypothesize that Sulphur Creek naturally attenuates the acid-sulfate geothermal components via a variety of processes.**

1.1. Geologic Background

The 1.2 Ma Valles Caldera in north-central New Mexico is a resurgent dome caldera located on the western margin of the Rio Grande Rift zone at the intersection of the Jemez Lineament and the Nacimiento Fault (Smith and Bailey, 1968; Goff and Gardner, 1994) (Figure 2). The Jemez Lineament is a NE-trending chain of volcanic centers, of which the

Jemez Volcanic Field is one, spanning from SE Arizona to NE New Mexico (Aldrich, 1986). The caldera rim spans a diameter of ~20-km. The eruptive history and regional stratigraphy were investigated during the drilling of the US DOE Continental Scientific Drilling Program core hole VC-2B (1762 m) in the Sulphur Springs area of the Valles resurgent dome (Gardner et al., 1989). Underlying the resurgent dome is >700 m of Quaternary debris flow and landslide deposits and eruptive material ranging in age from pre-caldera (~1.78 Ma) tuffs to caldera-associated tuffs (1.13 Ma) (Gardner et al., 1989; Goff and Gardner, 1994). Below these Quaternary volcanics is <100 m of Tertiary Santa Fe Group and ~700 m of Paleozoic sedimentary formations (Gardner et al., 1989; Goff and Gardner, 1994). The lower >200 m of core hole is in Precambrian basement rocks (Gardner et al., 1989; Goff and Gardner, 1994). Wilgus and others (2023) identify a low-shear velocities in a zone ~3-10 km below the surface beneath the Valles resurgent dome, corresponding to the location of the magma body that is the source of the geothermal heat in this system.

Goff and Janik, 2002 reported on the volatiles from the Valles geothermal system showing high He abundance and $^{3}He/^{4}He$, in addition to carbon dioxide and sulfur gases. Additional studies of the Valles-associated springs Soda Dam and Jemez Springs reproduced these $^{3}He/^{4}He$ compositions and suggested inclusion of deep endogenic fluids in their discharges, indicating a degree of mantle connectivity with agreement from regional studies of the Rocky Mountains (Karlstrom et al., 2013). This conclusion is consistent with the tectonic setting of the Valles Caldera at the intersection of the Rio Grande Rift and in a heavily faulted geologic setting that allows endogenic fluids to travel up to the surface (Figure 3).

Within the Sulphur Springs area, acquired by the National Park Service in 2020, acidic waters and volatiles emerge along local faults (Figure 3) in both discrete and diffuse features in both Sulphur and Alamo Canyons, suggesting faults serve as pathways for hydrothermal waters and gases to travel to the surface. The near-surface geology of the Sulphur Springs area is characterized by quaternary debris flows and landslide deposits exhibiting significant acid alteration and leaching (Goff and Gardner, 1994). This leaching is easily visible to the everyday observer as the ground surface is bleached near-white, shows buildup of salts, and is almost devoid of vegetation (Figure 4).

1.2. Hydrothermal Overview

The regional hydrothermal setting of the Valles Caldera is illustrated by the Goff and Janik (2000) model for a volcanic-hosted young igneous system. Soda Dam and Jemez Springs, in the Cañon de San Diego are representative of the distal neutral-pH chloride hot springs presented in the model, whereas the Sulphur Springs features are representative of the more centrally-located acid-sulfate springs and fumaroles presented in the Goff and Janik (2000) model (Figure 5).

Investigative core holes VC-2A and VC-2B (Figure 6) drilled during the US Department of Energy's Continental Scientific Drilling Program allow the overall Sulphur Springs acid-sulfate hydrothermal configuration to be assessed (Goff et al., 1988; Gardner et al., 1989; Goff and Gardner, 1994). In the subsurface (>600-700 m) beneath the Sulphur Springs area, hydrothermal fluids will exist in a liquid-dominated zone at temperatures in excess of 250 °C, but H_2O and H_2S will boil off at a depth approximately coincident with the 200 °C isotherm, creating a vapor zone (Figure 6) (Goff and Gardner, 1994). The vaporized H_2O and H_2S will condense in the few meters near the surface (Goff and Gardner, 1994).

When the fluids of the condensation zone reach the surface, the H_2S will oxidize to H_2SO_4 via the following simplified chain of reactions (Nordstrom et al., 2005):

$$(1) H^+ + 2HS^- + 2O_2 \rightarrow HS_2O_3^- + H_2O$$

$$(2) H^+ + S_2O_3^{2-} \rightarrow S^0 + HSO_3^-$$

$$(3) HSO_3^- + \frac{1}{2}O_2 \rightarrow SO_4^{2-} + H^+$$

This series of reactions will rapidly lower the pH of waters from the condensation zone from circumneutral to <3. More recently, workers have identified the role of micro-organisms in production of the sulfuric acid (Fernandes-Martins et al., 2023).

Sulphur Springs waters can be assessed using geochemistry from this and previous studies (Goff et al, 1985; Vuataz and Goff, 1986; Szynkiewicz et al., 2012) and are displayed in Figure 7). Sulphur Springs waters fall within a range from pH < 1 to pH > 4. Fluid temperatures at vents in the Sulphur Springs area range from 20 to 90^{0C}, with most samples falling between 40 and 60^{0C}. Steam collected from the Sulphur Springs fumarole has sulfate content of 4.5 mg/L (Goff et al, 1985). Liquid waters at vents have sulfate concentrations ranging from ~287 – 11,000 mg/L. Cl concentrations, however, range from below detection to 34 mg/L. The two highest Cl concentrations measured from a Sulphur Springs vent summarized here were measured in this study. The rest of the studies show Cl concentrations from below detection to ~ 8.6 mg/L. Stable isotopes of water in the geothermal area range from -80 to -40‰. The geothermal end-member at Sulphur Springs can be characterized as warm-to-hot, low-pH, high-sulfate waters with high concentrations of metals derived from leaching of the near-surface lithology (Goff and Gardner, 1994).

The acid waters formed from the H_2S oxidation geothermally alter near-surface landslide and debris flow deposits, with resultant phases including quartz, alunite, gypsum, kaolinite, and unspecified clays (Goff and Gardner, 1994). Solubility modelling for many of these and other phases is described later.

1.3. Hydrologic Overview

The headwaters of Sulphur Creek lie in the Valle Seco, north of the Valles resurgent dome (Figure 8). From its upstream extent until the confluence with Alamo Canyon, Sulphur Creek waters are of moderate pH and are fresh. Hydrothermal waters from the Alamo Canyon Fault are delivered to Sulphur Creek at the Alamo Canyon confluence. Further downstream, Sulphur Springs acid-sulfate features are the most significant source of low-pH hydrothermal waters along Sulphur Creek. Below the Sulphur Springs area, Sulphur Creek encounters the ephemeral drainage from Freelove Canyon. Under high-flow regimes, Freelove Canyon (ephemeral) routes fresh meteoric water into Sulphur Creek. Redondo Creek is the next confluence downstream, inputting moderately low- to neutral-pH waters. Below this confluence, the main channel retains the name of Redondo Creek. This naming convention differs between sources, but this thesis will refer to the channel as Redondo Creek downstream of the Sulphur – Redondo confluence. At its furthest downstream extent, Redondo Creek has a confluence with the circumneutral snowmelt- and monsoon-driven Rio San Antonio (Sherson, 2012). Sampling locations for this study are shown in Figure 8.

The hydrology of the Jemez River watershed for the study period is displayed in Figure 9 Stream discharge is mainly affected by melting of winter snowpack occurring in the mid-to-late spring and monsoonal precipitation occurring in the mid-to-late summer. Continuous discharge data for Sulphur Creek at selected sites (Figure 8) was accessed using

the National Park Service Integrated Resource Management Applications Portal. Jemez River discharge data at the Cañon gauge (downstream of the study area) was accessed through the USGS National Water Dashboard. Hydrologic data was assessed over an approximately two-year period from April 2021 to May 2023, encompassing all sampling dates from this project. Sulphur Creek and Jemez River gauging stations recorded the highest discharges of the study period in early April 2023, during peak snowmelt.

The Lower Sulphur Creek gauging station shows noticeably higher discharge than the Upper Sulphur Creek station due to its location downstream of the Sulphur Creek confluence with Alamo Canyon. The Jemez River gauge data was used to characterize the flow conditions of the Jemez watershed at large, and to compare study results with older datasets.

2. Methods

2.1. Field Methods

At each sample site (Figure 8) stream conditions were measured using an Oakton pH/Con 300 Series pH and conductivity meter. The pH probe was calibrated prior to each field excursion using pH 4, 7, and 10 standards. The conductivity probe was calibrated prior to each field excursion using a 1413 µS/cm standard solution. Sampling sites were organized as a system of triads at each significant stream confluence in the field area. Each confluence is comprised of three sample sites: a site on both stream reaches upstream of the confluence and one sample taken in the main channel downstream of the confluence. At each site, two water samples were collected. One sample was filtered through a 45 µm filter to remove sediment and was also acidified using concentrated nitric acid (HNO_3) to keep any metals dissolved in solution. The other sample bottle was collected with zero headspace to prevent

gas exchange so bicarbonate alkalinity analysis could be attempted in the lab. For selected samples near the Sulphur Springs area, hydrogen sulfide content of the water was assessed using a Hach hydrogen sulfide colorimetric test kit (Model HS-WR). For this assessment, each 25 mL water sample was acidified with 1 mL concentrated H_2SO_4 and 1 mL of potassium dichromate titrant was added. After a waiting period of 5 minutes, the titrated sample was transferred to a sample cell that was then compared to a titrated blank sample (DI water) using a color disc.

2.2. Lab Methods for Major ions and Stable Isotopes

Alkalinity analysis for this project was performed in the UNM Diagenesis Lab. Analysis method used was based on Michalowski et al. (2012). Major cation and anion compositions of collected water samples were analyzed in the UNM Analytical Chemistry Lab. Cation compositions were analyzed on the Optima 5300DV optical emissions spectrometer with a standard range of 2.5 – 10 mg/L. Major anion composition was analyzed on the Thermo Fisher/Dionex Ion Chromatography ISC 1100 ion chromatographer with a standard range of 2.5 – 20 mg/L. Major ion chemistry was analyzed using methods from Hou et al., 2000 and Jackson, 2000. Special methods were performed for ion chromatography analysis of samples with pH < 5 or high concentrations of chloride or sulfate. In this case samples were diluted with Na_2CO_3 eluent to neutralize pH prior to analysis. Multiple dilutions were analyzed for each sample and 10% of samples were analyzed in duplicate. Hydrogen and oxygen stable isotopes for collected water samples were analyzed in the UNM Center for Stable Isotopes using a Picarro L 1102-I Water Isotopic Analyzer, which utilizes cavity ring-down spectroscopy. Stable D and ^{18}O analyses were undertaken following a method from Wassenaar et al. (2012). Stable isotopic compositions of water are expressed in δ-notation, which is shown below:

$$\delta\ (‰) = \left(\frac{R_{sample}}{R_{standard}} - 1\right) * 1000$$

Where R_{sample} and $R_{standard}$ are $\frac{^{18}O}{^{16}O}$ or $\frac{^{2}H}{^{1}H}$ for the sample and the standard. The stable isotope standard used in this study was Vienna Standard Mean Ocean Water (V-SMOW).

Average analytical error for all analytes was calculated from duplicate samples. Average analytical error ±2.5% for cations, ±5% for anions. Analytical error for stable oxygen isotopes is ~±0.2‰ and for stable hydrogen isotopes is ~±1.5‰.

Elemental data for only aluminum, iron, chloride, and sulfate is discussed here as the focus of this study is on the sulfate emitted from the Valles acid-sulfate system as well as metal behavior in-stream. Data for other major ions are reported in Table 3.

2.3. Charge Balancing

Charge balancing was used in this study as a quality control check on major ion compositions. Charge balance error was calculated with the following equation,

$$Charge\ balance\ error\ (CBE) = \ 100 * \frac{\Sigma z_{cat} m_{cat} - \Sigma z_{an} m_{an}}{\Sigma z_{cat} m_{cat} + \Sigma z_{an} m_{an}}$$

where z_{cat} and z_{an} refer to the ionic charges of each cation and anion species respectively and m_{cat} and m_{an} refer to the concentration of each cation and anion species respectively expressed in mol kg^{-1}. As noted in studies of the Yellowstone geothermal system, waters with pH<3 tend to have negative charge balance errors, with lower pH values corresponding to more negative charge balance errors (Figure 10a). Adapting a method from Nordstrom and others (2009), who analyzed Yellowstone geothermal waters, inclusion of H^+ concentration in the charge balance calculation and distribution of total sulfate between the sulfate and bisulfate species provided improved low-pH charge balance errors (Figure 10b). Any

samples that fall outside the ±10% range after the sulfate modelling underwent a full geochemical speciation model in PhreeqC (Parkhurst, 1999), allowing pH to vary until neutral charge balance was achieved (Figure 10c; Table 1). This approach recognizes that the Oakton pH probe measures pH poorly below its calibration range at the low pH found in Sulphur Creek. Comparisons between pH measurements read from the Oakton meter and from pH paper are shown below (Table 2).

2.4. Radiogenic Strontium

Strontium isotopes were analyzed in the UNM Radiogenic Isotope Laboratory. 15-25 mL of filtered-acidified sample was used for analyses on a Thermo Neptune mc-ICP-MS. Samples were spiked with approximately 1 mL of UNM-Sr2 spike and then dried down on a hot plate to a moist paste. They were redissolved in 3N HNO_3 for Eichrom Sr-Spec resin column chemistry. Columns (2 ml) were prepped with 0.3 ml of resin, cleaned with ultrapure 18 MΩ water, and conditioned with 3N HNO_3. With the exception of Sr, the sample matrix was flushed through the columns using with 3N HNO_3, leaving strontium behind in the resin. The Sr was eluted with ultrapure 18 MΩ water , which was then dried down to a powder. The strontium powder was then redissolved in 0.5 mL of 3% HNO_3 and injected into the mass spectrometer.

2.5. Hydrology

Discharge data for three different gauging stations were obtained. Two of these sites (Upper Sulphur Creek, Lower Sulphur Creek) are on National Park Service property and are maintained by the NPS (Figure 8). Data for these two sites was obtained through the National Park Service Integrated Resource Management Applications Portal. Precision for the Sulphur Creek gauging stations is considered to be ±5% for the duration of this study. The third and final gauging station is on National Forest Service property and is maintained by the USGS.

The USGS Jemez River gauge is located downstream of the field area of this study (Figure 1) and is used as an estimator of regional flow conditions. Data for this site was obtained through the USGS National Water Dashboard application. Both data sources are publicly available. Data was obtained for the 10-year time period extending from May 2013 to May 2023 to determine long-term discharge patterns.

2.6. Geochemical Modelling

Geochemical modelling was undertaken using USGS PhreeqC (Parkhurst, 1999) and The Geochemist's Workbench (Bethke, 2021). Modelling was carried out for the purpose of understanding likely geochemical speciation and mineral saturation. Where a model-required constraining parameter was not available, the PhreeqC default value was used. Geochemical modelling relies on determining the composition of a solution relative to thermodynamic equilibrium for a range of reactions.

3. Results

Field parameters, major ion, and isotope compositions of all samples are reported in Table 3.

3.1. Field Parameters

Field parameters for this study were collected at each sampling site, consisting of temperature, pH, conductivity, and total dissolved solids (TDS). Here, pH and conductivity trends are discussed.

pH in the field area for this study is generally bimodal (Figure 11). The first cluster of pH-values falls between pH 2-3.5, generally corresponding to waters in the Sulphur Creek

drainage downstream of the confluence with the Alamo Canyon drainage and upstream of the Redondo Creek confluence (Figure 8). The second cluster of pH-values falls between approximately pH 5-6.5, generally corresponding to waters in the Sulphur Creek drainage upstream of the confluence with the Alamo Canyon drainage and various dilute tributaries such as the Freelove Canyon drainage and the Río San Antonio.

Conductivity (µS/cm) does not show such a clear bimodality, but in-stream conductivity measurements are generally low upstream of Sulphur Springs, see their high values at Sulphur Springs, and decrease downstream of Sulphur Springs (Figure 12). Conductivity values for samples in this study range from 75 (µS/cm) to >12,000 (µS/cm).

3.2. Major Ions

Major ions analyzed for this sample were calcium, magnesium, sodium, potassium, chloride, and sulfate. Additionally, aluminum, iron, and manganese are reported. Major ion compositions are reported as total mg/L in Table 3. Measured aluminum concentrations range from 0 mg/L (below detection; ~0.1 mg/L by the methods used) up to >800 mg/L. Sulfate concentrations range from 8 mg/L to >11,000 mg/L. Most major ions have their peak concentration at a Sulphur Springs vent, with a few exceptions. Due to the low-chloride nature of acid-sulfate springs, peak chloride concentrations are found in Redondo Creek upstream of the Sulphur Creek confluence. Peak bicarbonate (HCO_3^-) concentrations are found in the Freelove Canyon drainage upstream of the Sulphur Creek confluence, as the low pH found in the Sulphur Creek watershed means that the predominant carbonate species is fully-protonated carbonic acid (H_2CO_3) and therefore were not determined by the methods used in the study.

3.3. Dissolved Sulfide

Dissolved sulfide (S^{2-}) concentrations of geothermal features ranged from 1.15 – 1.95 mg/L. Where measured, in-stream concentrations of sulfide tend to be below detection via the Hach colorimetric method. However, for a small reach of Sulphur Creek (<50 m) immediately adjacent to the Sulphur Springs area, in-stream dissolved sulfide concentrations are measurable (ranging from 0.06 – 1.10 mg/L).

3.4. Stable Isotopes

Stable isotope compositions of sample waters are reported in Table 3 (Figure 13). $\delta^{18}O$ values for waters ranged from -15‰ to -1‰. δD values for waters ranged from -86‰ to -40‰. Waters are plotted with reference to the global meteoric water line (GMWL) of Craig (1961).

3.5. Strontium Isotopes

Strontium concentrations analyzed in the ICP-OES range from <0.01 to 1.87 mg/L (Table 4). From all study samples, 8 were selected for Sr-isotope analysis. Sr concentrations for these selected samples were measured again this time using the ICP-MS during isotopic analysis. These mass spectrometer-derived concentrations range from 0.04 to 1.81 mg/L (Table 4). $^{87}Sr/^{86}Sr$ values for these samples range from 0.707688 to 0.711529.

3.6. Geochemical Modelling

Geochemical speciation and saturation modelling for this study was undertaken using USGS PhreeqC (Parkhurst, 1999). Model results are reported in Table 5. Minerals selected for reporting in this study are those aluminum-, iron-, and/or sulfate-bearing minerals that might attenuate these components.

4. Discussion

4.1. Stable Isotope Chemistry

Stable $\delta^{18}O$ and δD values of sampled waters are shown in Figure 13. Most stream samples fall along the Global Meteoric Water Line (Craig, 1961) or the Local Meteoric Water Line for the Jemez Mountains (Vuataz and Goff, 1986), indicating a dominant meteoric origin for a majority of the stream water samples collected for this study. Stable $\delta^{18}O$ and δD values of samples collected match up very well to values reported in previous studies (Vuataz and Goff, 1986; Szynkiewicz et al., 2012), plotted in grey in Figure 13, and in fact extend the range of possible acid-sulfate springs compositions to include isotopically heavier waters.

Samples collected from Sulphur Springs and a small number of stream samples fall off the LMWL. Samples collected from the Men's Bathhouse Mudpot and a small number of stream samples collected in the Alamo Canyon drainage fall below and to the right of the LMWL, which is interpreted as an evaporation effect, which preferentially leaves ^{18}O- and D-bearing water molecules (Vuataz and Goff, 1986). This interpretation is consistent with each site and observed water vapor discharge. Hydrothermal waters are discharged at Men's Bathhouse Spring at temperatures of 38-82 °C (Vuataz and Goff, 1986; Sznynkiewicz et al., 2012), which suggests that the stable isotope trend seen in the mudpot is due to loss of water vapor at the surface (Figure 14a). This evaporation trend at the Men's Bathhouse Mudpot is matched in previous studies (Vuataz and Goff, 1986; Sznynkiewicz et al., 2012). The evaporation trend from stream waters in the Alamo Canyon drainage is consistent with the boggy canyon floor conditions and frequent ponding of stream waters (Figure 14b).

Water samples collected from other major vents in the Sulphur Springs area fall off the line above and to the left of the LMWL. Two samples of steam from the main Sulphur Springs fumarole collected and assessed by Vuataz and Goff (1986) are interpreted by these investigators as the residual component of the evaporation trend from the ^{18}O-enriched waters of the Men's Bathhouse Mudpot. Two other samples collected at the Footbath Spring vent (18-39 °C) by Vuataz and Goff (1986) fall off the LMWL by about 10‰. The displacement of these samples along the $\delta^{18}O$-axis is interpreted by these investigators to be caused by enhanced ^{18}O-fractionation between H_2O and aqueous CO_2 at lower temperatures. For this reason, the samples collected for this study at the Women's Bathhouse Spring and Lemonade Spring vents are more likely related to the evaporation trend seen between the fumarole waters and the mudpot waters due to their higher temperatures (32-89°C). Even though the temperature at Women's Bathhouse at time of collection (32°C) overlaps with the range of temperatures collected at Footbath Spring in previous studies, the ^{18}O-displacement of the Women's Bathhouse sample is not nearly as large as those at Footbath Spring, which suggests a different process besides CO_2-fractionation affecting its isotopic composition. The CO_2-fractionation hypothesis from Vuataz and Goff (1986) is supported by Smith (2019) who measured CO_2-flux at Sulphur Springs (Table 6). CO_2 flux at Men's Bathhouse is noticeably higher than at Women's Bathhouse and Lemonade Spring (referred to in Smith (2019) as Lemon Spring), but the proposed fractionation from Vuataz and Goff (1986) relies on lower fluid temperatures to achieve the magnitude of fractionation seen at Footbath Spring. The temperature at Men's Bathhouse in this conceptual model would inhibit CO_2-water fractionation, while the low CO_2-flux at Women's Bathhouse and Lemonade Springs would inhibit fractionation at these vents.

4.2. Field Parameters

Each sample in this study was collected alongside a suite of field parameters: pH, temperature, electrical conductivity, and total dissolved solids (TDS). Electrical conductivity and pH display a negative relationship (Figure 15). Low-pH, high-conductivity hydrothermal waters originating from Sulphur Springs become fresher as the pH increases. Any process that removes ions from solution (e.g. precipitation, sorption, cation exchange) would reduce the electrical conductivity of the solution, as would dilution with fresh water. It follows that this negative trend between electrical conductivity and pH illustrates the sum of all ongoing attenuation processes: any process that attenuates aqueous ions contributes to this trend with or without dilution.

4.3. Aluminum, Sulfate, Iron, and Strontium

Maps detailing spatial variations in geochemistry are included in Appendix 1.

Aluminum

As a metal, aluminum is exceptionally sensitive to changes in in-stream pH-conditions. Figure 16 shows the relationship of in-stream aluminum concentrations to pH. At lower pH, in-stream aluminum concentrations are higher and generally decrease with increasing pH. Very little aluminum is detectable above pH 4 and no aluminum is detectable above pH 5.5. This is largely consistent with previous research regarding aluminum solubility in acidic environments. Nordstrom and Ball (1986) studied aluminum solubility in acidic solutions and found that it behaves conservatively ~ pH < 4.5 and non-conservatively at pH > 5. Non-conservative aluminum behavior is suggested by previous researchers

(Nordstrom and Ball, 1986; Bigham and Nordstrom, 2000; Jones et al., 2011) to be controlled by precipitation of gibbsite ($Al(OH)_3$) or amorphous $Al(OH)_3$ occurring at the first hydrolysis of aluminum:

$$Al^{3+} + H_2O \leftrightarrow AlOH^{2+} + H^+ \quad (pK_1 = 5)$$

While aluminum concentrations for the Sulphur Creek field area are variable, they do display a trend of decreasing concentration with increasing pH. Geochemical modelling with PhreeqC indicates that only three samples assessed in this study are supersaturated with respect to gibbsite ($Al(OH)_3$) and no samples are supersaturated with respect to amorphous $Al(OH)_3$ (Table 5). This implies the primary control on aluminum concentrations in the field area is dilution as aluminum behaves conservatively at pH < 4.5 (Nordstrom and Ball, 1986). Most samples at pH > 5 have aluminum concentrations below detection, which make it difficult to quantify hydroxide precipitation. However, the shift from conservative to non-conservative aluminum behavior in the pH 4.5-5 transition zone is observed in other acid-sulfate environments (Bigham and Nordstrom, 2000). ICP-MS analyses of metal concentrations would be required to resolve the behavior of aluminum at these low concentration at pH >5 and may be grounds for thorough investigation in future studies.

Figure 17 displays the relationship between aluminum and chloride concentrations. This plot displays three different trends in the Al-Cl ratio. The first is a positive trend between aluminum and chloride concentrations seen in the upper Sulphur watershed between Alamo Canyon and Redondo Creek confluences with Sulphur Creek. This stretch of Sulphur Creek is predominantly at pH < 4, which suggests conservative aluminum behavior. Indeed, several samples downstream of Sulphur Springs lie along an apparent mixing line between

waters from Sulphur Springs and Alamo Canyon ("Sulphur-Alamo Spring/Summer" line in Figure 17).

The second trend is an approximately flat trend in which Al varies little and Cl increases. This trend is made up of samples taken from the fresh tributaries in the field area ("Redondo Trend" line in Figure 17). This trend is characterized by samples with pH ~ 4-7, which suggests that Al should behave non-conservatively through some of this stretch. The four samples modelled by PhreeqC to be supersaturated with respect to alunite (boldly outlined) lie along this trend, which adds support to the hypothesis that mineral precipitation is responsible for some degree of Al-attenuation. No precipitates were observed forming in the course of this work, but anecdotal evidence and VCNP photo archives suggest that under some conditions, a milky precipitate in the stream has been observed at confluences in the Sulphur watershed.

The two samples that fall off either trend were collected in October 2021 and are from sampling locations downstream of Sulphur Springs and upstream of Freelove Canyon. As neither of these samples are modelled to be supersaturated with respect to any Al-bearing minerals, we hypothesize that this could be a third trend ("Sulphur Alamo Fall/Winter" in Figure 17) due to seasonal variability in the composition of Sulphur Springs, which would change the mixing trend between Sulphur Springs and Alamo Canyon. Samples from the Alamo Canyon, Sulphur Creek near the springs, and Freelove Canyon confluences tend to show higher Cl concentrations than their analogous spring/summer samples (Figure 17). This could be true of Sulphur Springs as well, and seasonal variability of concentrations from Sulphur Springs vents is reported by other investigators (Vuataz and Goff, 1986;

Szynkiewicz et al., 2012). This variation in composition could explain the two October 2021 samples as mixtures of waters that vary seasonally.

Notably in Figure 17 is the trend of increasing Cl downstream in the watershed (blue triangular data points representing samples from the Redondo – San Antonio confluence), indicating that Cl is being added, not diluted: thus does not behave conservatively in this part of the study site. The cause of this non-conservative behavior is speculated to be due to localized land-use: private land near the Sulphur – Redondo confluence is used for agricultural purposes, including cattle grazing, which could be contributing elevated Cl concentrations via dissolution of salt licks intended for cattle consumption.

Figure 18 shows a series of four plots of aluminum, iron, sodium, and sulfate versus chloride content in mmol/L in the field area. The Na-Cl subplot shows two mixing trends, one of which is marked by a red line, noting the 1:1 mixing line, suggesting these waters lower in the watershed at the Sulphur – Redondo and Redondo – San Antonio confluences are potentially affected by halite dissolution. Whether this is a geologic or anthropogenic source is currently unknown. It is apparent, then, that chloride cannot be used as a conservative tracer at these confluences in the watershed. The upstream regions of Sulphur Creek can and do show conservative chloride behavior.

Since Li concentrations are not great enough in this watershed to be detected with ICP-OES methods, δD will be used as a conservative tracer for the whole watershed. Here, each sample has a unique isotopic signature that can be used to trace mixing of waters. When samples are differentiated by dates for which a full suite of data were collected (11/10/2021, 8/3/2022, 10/12/2022, 5/16/2023), some interesting trends appear in the Al- δD relationships (Figure 19). Al-bearing water samples appear to display conservative mixing trends and

generally hold linear relationships with the isotopic composition of the waters. There are a few exceptions to these linear relationships, those being waters from Alamo Canyon and waters emitted from Sulphur Springs. Waters from Alamo Canyon undergo evaporation at the surface, which lead to isotopically heavier compositions. Sulphur Springs waters undergo a variety of processes that lead to isotopically heavier signatures (see section 4.1). For each of the sampling dates displayed in Figure 19, where all three samples of a triad have measurable Al-content, the downstream sample tends to fall on a line between the compositions of the upstream samples. In the 8/3/2022 sampling date (Figure 19), the Redondo Creek sample collected above the Sulphur – Redondo confluence is modelled to be supersaturated with respect to alunite, but the sample collected downstream of the confluence does not fall cleanly on a line between the two upstream samples, which suggests that non-conservative processes occurred at this site on this date.

Previous studies focusing on the Sulphur Springs area (Goff et al., 1985; Goff and Gardner, 1994) and the Yellowstone geothermal system (McCleskey et al., 2010b) report noticeable concentrations of fluoride in geothermal spring waters (2.73 – 5.2 mg/L). McCleskey and others (2010b) emphasize the importance of fluoride complexation in retaining Al in solution, with an estimated >70% of the aqueous Al load in the Gibbon River existing as an Al-F complex. Very few samples in this study had detectable F and those that did had concentrations that fell below the standard range for ion chromatography (2.5-20 mg/L). For this reason, F was not considered in this study nor was it used in charge balancing calculations. However, with more accurate analysis, the role of F in Al solubility for the Sulphur Creek system can be further developed.

Sulfate

Sulfate (SO_4^{2-}) is the primary aqueous anion in the Sulphur Creek system. High SO_4 concentrations in this system originate from surface oxidation of magmatic H_2S derived from the Valles magmatic system (Goff and Janik, 2000; Szynkiewicz et al., 2019). SO_4 concentrations in the Sulphur Creek watershed find their highest in-stream levels just downstream of the Sulphur Springs area. Figure 20 shows a plot of log SO_4 concentrations vs pH. This is an approximately linear relationship, with SO_4-values clustering together at low-pH and showing more variability at circumneutral pH. The highest SO_4 concentrations are found at low pH, which is consistent with SO_4 acting as the primary aqueous ion and related to acidity in the acid-sulfate geothermal system (via the chemical equations shown earlier).

As with Al, SO_4- δD relationships were assessed. Similar relationships are observed in SO_4- δD space. The downstream sample at each confluence generally falls between the two upstream samples, indicating conservative mixing at these confluences. However, boldly outlined data points in Figure 21 show samples modelled to be supersatured with respect to alunite. Note that the Sulphur – Redondo cluster on 8/3/2022 shows the same general relationship as in Al. Interestingly, the Redondo – San Antonio cluster for 10/12/2022 contains an upstream sample that has modelled alunite supersaturation, but the downstream sample lies on a conservative mixing line between the two upstream samples. This could be due to the fact that Río San Antonio has such a higher discharge than Redondo Creek that any geochemical evidence of non-conservative mixing is washed out.

Iron

Iron concentrations in the Sulphur Creek watershed range from below detection to >150 mg/L. Aqueous Fe concentrations do not appear to be as sensitive to the first hydrolysis of Fe^{3+} as is Al (Figure 22). The hydrolysis constants for Fe^{3+} are as follows (taken from Nordstrom et al., 2009):

$$Fe^{3+} + H_2O \leftrightarrow FeOH^{2+} + H^+ \quad pK_1 = 2.19$$

$$FeOH^{2+} + H_2O \leftrightarrow Fe(OH)_2^+ + H^+ \quad pK_2 = 3.48$$

$$Fe(OH)_2^+ + H_2O \leftrightarrow Fe(OH)_3^0 + H^+ \quad pK_3 = 6.93$$

Fe concentrations are highest at low-pH and trend downward with increasing pH in a similar manner to Al. Most samples with measurable Fe concentrations tend to fall between pH = pK_1 and pH = pK_2, however, there do not appear to be changes in slope at each of these pH values. Fe concentrations are generally below detection at pH > pK_2, however five samples retain measurable Fe concentrations above this threshold (Table 5). Geochemical modelling performed in PhreeqC indicates that these five samples are supersaturated with respect to goethite (FeOOH). Of all samples with measurable Fe concentrations, those modelled to be undersaturated with respect to goethite occur at pH < pK_2 and those modelled to be supersaturated with respect to goethite occur at pH > pK_2.

Given the lack of redox parameters for samples collected in this study, the Fe system is difficult to quantify. Bigham and Nordstrom (2000) stress the significance of ferrihydrite ($Fe_2^{3+}O_3 \cdot 0.5H_2O$) and schwertmannite ($Fe_8O_8(OH)_{8-2x}(SO_4)_{x(s)}$) in controlling iron concentrations in acid-sulfate environments. However, PhreeqC geochemical models do not

even consider ferrihydrite and schwertmannite for these samples, presumably due to the very low (~10^{-10} mol/kg) concentrations of Fe^{3+} calculated by the software.

Fe-δD relationships are displayed in Figure 23 and bear resemblance to the Al- and SO_4- relationships with δD. The 8/3/2022 Sulphur – Redondo cluster shows the same relationships, but this time the boldly outlined points show modelled supersaturation with respect to goethite, which is an Fe-oxyhydroxide. The fact that this sample shows goethite supersaturation and the downstream sample of this triad shows a similar deflection from conservative mixing between the tributaries suggests that non-conservative processes were occurring at this sample site on that date.

Strontium

Strontium isotopes and concentrations for selected samples are compared in Figure 24. Two samples from Sulphur Springs have $^{87}Sr/^{86}Sr > 0.711$, while the rest (one Sulphur Springs sample and five stream samples from three different confluences) have $^{87}Sr/^{86}Sr < 0.709$. These two values correspond to Sr isotope ratios found in the Lower Bandelier Rhyolite Pumice and an unspecified rhyolite unit (Vuataz et al., 1988). However, the Sulphur Springs samples are potentially affected by mixing between waters bearing the Sr-signatures of several different lithological units. The surface water samples included in the Sr analyses cannot be simply categorized by lithological units as their Sr compositions may be influenced by subsurface *and* Sr accumulated along surface flow paths. Sr isotopes for Sulphur Creek waters would require further investigation to determine the source of Sr signatures in surface

streams. However, the $^{87}Sr/^{86}Sr$-values for Sulphur Springs are in agreement with those reported by Vuataz and others (1988) and are significantly lower than the reported isotopic ratio reported for Precambrian basement rocks beneath the caldera (0.7569, also reported in Vuataz et al. (1988)).

4.4. Hydrology

Hydrographs for all three gauging stations in the field area are displayed in Figure 9 and gauge summaries in Table 7. Stream discharge followed a typical pattern, seeing discharge peaks during spring snowmelt events and in the late summer during monsoonal precipitation. Discharge at these gauges for the duration of the study generally remained around 10-year median levels. However, melting of snowpack in spring 2023 led to 10-year maximum discharges in Sulphur Creek and the Jemez River. The maximum discharges at each gauge ranged from 50 – 110 times the 10-year median discharge.

For this study, discharge data was not readily available along the whole length of Sulphur Creek and associated tributaries. Daily average discharge at the Lower Sulphur Creek HOBO was used as a proxy value for discharge in the field area and compared to *in-stream* (spring chemistry omitted as it is less affected by discharge) concentrations of Al, Fe, and SO_4 for sampling dates (Figure 25). In this figure, discharge data is used as a categorical variable to describe the general flow conditions in the Sulphur Creek watershed. Samples collected on high-discharge days tend to show lower solute concentrations.

Of the three contaminants discussed here, sulfate concentrations show the strongest relationship to discharge. Under higher discharge conditions, a larger number of each samples in each suite (and therefore a larger stream reach) had SO_4 concentrations below the

Secondary MCL. The lower discharge sample suites tend to have more samples above the MCL, but this is due to smaller sample suites concentrated in Sulphur Creek, which would skew the median concentration to higher levels and not account for downstream concentrations. The sulfate precipitate that is seen coating the gravel around the Sulphur Springs area may re-dissolve during high-discharge events, which would increase the total SO_4 load even if the concentration was significantly lower due the higher discharge.

Aluminum concentrations are evidently not as closely controlled by discharge. The two highest-discharge suites show the smallest spreads of concentration (as expected), however, the two lowest-discharge suites have similarly low median concentrations to the high-discharge suites (which is the reverse of the SO_4 situation). As with SO_4, this is likely partly due to a smaller samples size for the corresponding dates. Another complexity to assessing the role of discharge is analytical. In-stream Al concentrations are significantly lower than SO_4 concentrations, which means that higher discharge regimes result in more dilute Al concentrations, some of which will be undetectable or below the standard range for ICP-OES. This would skew the spread of Al data to higher concentrations as the most dilute samples cannot be considered.

4.5. Loading Estimates

In-stream solute load calculations are useful for investigating trends and processes for these solutes while accounting for discharge conditions (Kimball et al., 2010). The mass-loading approach allows investigators to characterize solute sources decoupled from concentrations using longitudinal synoptic sampling. One of the basis assumptions in the mass-loading approach is that hydrologic conditions remain constant on the sampling day, which implies that changes in solute mass loads are due to inputs (losses) from different

sources (sinks) rather than a change in overall hydrologic conditions (Kimball et al., 2010). Solute mass loads in Sulphur Creek are estimated below. Due to the small overall size of the field area for this study, discharge measurements are sparsely distributed over the field area, which makes mass-load calculations difficult. However, previous studies focusing on mass-loading in the Jemez watershed (Dyer, 2007; Golla, 2019) are used to provide tentative estimates of changes in solute mass-load downstream of the field area.

Solute loading in Sulphur Creek is calculated using the method set forward in Dyer (2007). Solute load is calculated as:

$$Load\ [mg\ s^{-1}] = Q\ [L\ s^{-1}] * C_i\ [mg\ L^{-1}]$$

where Q = discharge at the nearest gauge and C_i = concentration of solute i. The Upper Sulphur Creek gauge provides discharge for samples taken from Sulphur Creek upstream of Alamo Canyon. The Lower Sulphur Creek gauge is used to obtain discharge for samples taken from Sulphur Creek downstream of Alamo Canyon. Where available, the now-defunct Sulphur Creek Flume was used to get discharges for sample taken from Sulphur Creek downstream of Sulphur Springs. In order to estimate load downstream of the field area, one load estimate for Rio San Antonio upstream of from Dyer (2007) was taken. Results of loading calculations are shown in Table 8. Across 5 different sampling dates, Al loads ranged from ~2 mg/s to ~390 mg/s. Fe loads ranged from ~6 mg/s to ~170 mg/s. SO_4 loads ranged from ~430 mg/s to ~11,000 mg/s. Mn was undetectable for all samples sites for which there was discharge data.

There is one standalone sample that had an associated discharge for the collection date, but none of the adjacent samples on that campaign had appropriate discharge data and

so were omitted from loading calculations. Three campaigns (8/3/2022, 10/12/2022, 5/16/2023) had available discharge data for the Upper and Lower Sulphur Creek gauges and only the 10/12/2022 campaign had viable discharge data from the Sulphur Creek flume as well. For two of the campaigns (11/10/2021, 8/3/2022), mass-loading estimates from previous studies (Dyer, 2007; Golla, 2019) were used on the basis of similar discharge at the USGS Jemez River gauge..

Sulfate loading into Sulphur Creek from Alamo Canyon ranges from ~5000 mg/s to ~10,500 mg/s (Table 8; corresponding to a ~580 - ~1800% increase). The only sample with viable accompanying discharge from the Sulphur Creek Flume suggests SO_4 loading into Sulphur Creek of ~1500 mg/s (corresponding to a 26% increase) originating from Sulphur Springs.

Previously reported data from the Gibbon River in Yellowstone National Park indicate much higher Fe and SO_4 loading due to interaction with low-pH geothermal waters of Yellowstone's Norris Geyser Basin. Data reported by McCleskey and others (2010a, 2010b) results in maximum Fe and SO_4 loads of ~440 and ~40,500 mg/s respectively. The respective maximum Fe and SO_4 loads for Sulphur Creek are ~160 and ~11,000 mg/s. Al loading is comparable between the Valles and Yellowstone geothermal systems. This study returns a maximum Al load of ~390 mg/s, while the maximum for the Yellowstone study is ~490 mg/s (Table 8).

The discrepancy between SO_4 and Al loading between Valles and Yellowstone can potentially be explained by way of considering the source of the acid-sulfate waters in both volcanic systems. SO_4 content of acid-sulfate and geothermally-affected waters is derived from sulfur degassing from the magma body underlying each volcano separately, whereas

Al- and Fe-compositions of these waters are derived from leaching of near-surface rocks within the acid-condensation zone (Goff and Gardner, 1994). In this way, the discrepancy between SO_4 loading between Yellowstone and Valles can be considered a proxy for the difference in sulfur degassing from the respective magma bodies, while the Al loading similarity can be a function of similar near-surface rock compositions. Another consideration is that the immediate vicinity of the Sulphur Springs area was heavily anthropogenically disturbed in the process of constructing the settling pond, which could enhance Al leaching from the surrounding landscape.

4.6. Water Quality Implications

The U.S. EPA includes Secondary Drinking Water Maximum Contaminant Levels (MCL) of 0.2 mg/L, 0.3 mg/L, and 250 mg/L for Al, Fe, and SO_4 respectively (EPA, 2023). A majority of stream samples collected in this study have Al and Fe concentrations in excess of their MCL. At the downstream extent of the field area (Río San Antonio downstream of the Redondo Creek Confluence), very little Al and Fe remains in solution. However, a majority of samples collected in this study are in excess of the MCL, regardless of discharge conditions. A significant number of samples fall below the MCL for SO_4, with the discharge conditions apparently controlling how far upstream the concentrations drop below MCL. A greater number of stream samples (and therefore a larger stream reach) fall below the SO_4 MCL under higher discharge regimes (Figure 25).

The Al EPA Secondary MCL is 0.2 mg/L, which adds a layer of complexity to identifying water quality implications. The 0.2 mg/L concentration is significantly below the ICP-OES standard range (2.5 – 10 mg/L). Without more accurate low-concentration

methods, it is difficult to exactly identify whether Al has been attenuated to a level below the Secondary MCL.

Geographic representations of water quality are displayed in Figure 25. Samples collected upstream of Sulphur Springs have either dilute or undetectable concentrations of Al and SO_4 and moderate- to neutral-pH. Upon interaction of Sulphur Creek with acid-sulfate waters from the Sulphur Springs area, high-Al and SO_4 signatures are found in-stream as well as low pH. In general, Sulphur Creek is most impacted in the reach downstream of Sulphur Springs, but upstream of the Redondo – San Antonio confluence. At this site, samples are generally quite dilute and circumneutral in pH. Breakdowns of each map for Al, SO_4, Fe, and pH for the four sample dates with a full suite of samples collected are presented in Appendix A.

5. Conclusions

The Sulphur Creek watershed is an example of a self-scrubbing system in which geochemical and hydrologic factors combine to remove selected geothermal components from solution. This study highlights the significance of mixing between geothermal waters and fresh meteoric waters in attenuating geothermal components. The resulting pH change from this mixing is likely responsible for metal attenuation via hydrolysis. Geochemical modelling suggests that several samples are supersaturated with respect to Al-, Fe-, and SO_4-bearing minerals, even though in-stream precipitation of these minerals was not observed during field campaigns). While in-stream precipitation was not observed, mineral crusts in the Sulphur Springs area are evident and have been characterized by previous studies (Goff and Gardner, 1994). Samples modelled to be supersaturated with respect to these minerals

are moderate in pH and relatively dilute with respect to these solutes. They also have variable Cl-compositions, usually as a result of mixing with higher-Cl tributaries. The role of mixing with dilute freshwater is supported by stable isotope analysis, which shows the reduction in SO_4 concentrations in selected samples with lower δD (greater meteoric fraction).

Studies from Yellowstone suggest that sorption in geothermally-affected streams is not likely to be a significant attenuation process, due to the formation of silica coatings on suspended sediments (McCleskey et al., 2010a). As in Yellowstone, amorphous silica saturation is prevalent in the Sulphur Creek watershed. Yellowstone comparisons are also able to be made via loading estimates for Sulphur Creek versus the Gibbon River (McCleskey et al., 2010a; McCleskey et al., 2010b). Sulfate loading in the Gibbon River is noticeably higher than in Sulphur Creek. However, Sulphur Creek is the primary flowpath for acid-sulfate geothermal waters, whereas the context of Gibbon River loading relative to the rest of the Yellowstone system is unclear.

Discharge patterns also affect attenuation. Under a low-flow regime, a greater proportion of Sulphur Creek water is derived from acid-sulfate spring water originating from Sulphur Springs. At higher flows, a greater proportion of Sulphur Creek water is derived from fresh meteoric water and will dilute geothermal components more effectively. For less pH-sensitive solutes like SO_4, a clear negative relationship between concentration and discharge appears, emphasizing dilution in SO_4-attenuation. pH-sensitive solutes like Al and Fe do not show as clear of a negative relationship, although the statistical spread of concentrations generally decreases at higher flows.

In summary, this project has provided 68 new water analyses for the Sulphur Creek and downstream watersheds and has provided insight into the processes of dilution and

precipitation in removing geothermal components and neutralizing pH. With the recent acquisition of the Sulphur Springs area by the National Park Service, extreme water chemistry should be taken into account as the area becomes subject to higher visitation. Research into the Sulphur Springs geologic system also helps bring more understanding to this wonderful natural feature and other places like it.

References

Aldrich, M.J., 1986, Tectonics of the Jemez Lineament in the Jemez Mountains and Rio Grande Rift: Journal of Geophysical Research, v. 91, p. 1753-1762.

Bethke C. M., 2021, The Geochemists Workbench: University of Illinois.

Bigham, J.M., and Nordstrom, D.K., 2000, Iron and Aluminum Hydroxysulfates from Acid Sulfate Waters: *Reviews in mineralogy and geochemistry*, v. 40, p. 351-403

Craig, H., 1961b, Isotopic Variations in Meteoric Waters: Science, v. 133, p. 1702-1703.

Dyer, J., 2007, Groundwater-Surface Water Interactions: Effects of Geothermal Spring Inputs to Jemez River Water Quality [M.W.R Thesis]: University of New Mexico, 39 p.

EPA, 2023, Secondary Drinking Water Standards: Guidance for Nuisance Chemicals, 2023: https://www.epa.gov/sdwa/secondary-drinking-water-standards-guidance-nuisance-chemicals (accessed June 9 2023).

Fernandes-Martins, M.C., Colman, D.R., and Boyd, E.S., 2023, Relationships between fluid mixing, biodiversity, and chemosynthetic primary productivity in Yellowstone hot springs: Environmental Microbiology, v. 25, p. 1022-1040.

Gardner, J.N., Hulen, J.B., Lysne, P., Jacobson, R., Goff, F., Nielson, D.L., Pisto, L., Criswell, C.W., Gribble, R., Meeker, K., Musgrave, J.A., Smith, T., Wilson, D., 1989, Scientific Core Hole Valles Caldera #2b (VC-2B), New Mexico: Drilling and Some Initial Results: OSTI Report LA-UR-89-2025, 10 p.

Goff, F. and Gardner, J.N., 1994, Evolution of a Mineralized Geothermal System, Valles Caldera, New Mexico: Economic Geology, v. 89, p. 1803-1832.

Goff, F., Gardner, J., Vidale, R., and Charles, R., 1985, Geochemistry and Isotopes of Fluids from Sulphur Springs, Valles Caldera, New Mexico, v. 23, p. 273-297.

Goff, F. and Janik, C, 2000, Geothermal Systems: Encyclopedia of Volcanoes, p. 817-834.

Goff, F. and Janik, C.J., 2002, Gas geochemistry of the Valles caldera region, New Mexico and comparisons with gases at Yellowstone, Long Valley, and other geothermal system: Journal of Volcanology and Geothermal Research, v. 116, p. 299-323.

Goff, F., Shevenell, L., and Gardner, J.N., 1988, The Hydrothermal Outflow Plume of Valles Caldera, New Mexico, and a Comparison With Other Outflow Plumes: Journal of Geophysical Research, v. 93, p. 6041-6058.

Golla, J.K., 2019, Natural Salinization of the Jemez River, New Mexico: An Insight from Trace Element Geochemistry [M.S. thesis]: University of New Mexico, 62 p.

Hou, X., and Jones, B.T., 2000, Inductively Coupled Plasma/Optical Emission Spectrometry: Encyclopedia of Analytical Chemistry, p. 9468-9485.

Jackson, P.E., 2000, Ion chromatography in environmental analysis: Encyclopedia of Analytical Chemistry, p. 2779-2801.

Jones, A.M., Collins, R.N., and Waite, D.T., 2011, Mineral species control of aluminum solubility in sulfate-rich acidic waters: *Geochimica et Cosmochimica Acta*, v. 75, p. 965-977.

Karlstrom, K.E., Crossey, L.J., Hilton, D.R., Barry, P.H., 2013, Mantle ^{3}He and CO_2 degassing in carbonic and geothermal springs of Colorado and implications for neotectonics of the Rocky Mountains: Geology, v. 41, p. 495-498.

Kimball, B.A., Runkel, R.L., and Walton-Day, K., 2010, An approach to quantify sources, seasonal change, and biogeochemical processes affecting metal loading in streams: Facilitating decisions for remediation of mine drainage: Applied Geochemistry, v. 25, p. 728-740.

McCleskey, R.B., Nordstrom, D.K., Susong, D.D., Ball, J.W., Holloway, J.M., 2010a, Source and fate of inorganic solutes in the Gibbon River, Yellowstone National Park, Wyoming, USA: I. Low-flow discharge and major solute chemistry: Journal of Volcanology and Geothermal Research, v. 193, p. 189-202.

McCleskey, R.B., Nordstrom, D.K., Susong, D.D., Taylor, H.E., 2010b, Source and fate of inorganic solutes in the Gibbon River, Yellowstone National Park, Wyoming, USA. II. Trace element chemistry: Journal of Volcanology and Geothermal Research, v. 196, p. 139-155.

McGibbon, C., Crossey, L.J., Karlstrom, K.E., Grulke, T., 2018, Carbonic springs as distal manifestations of geothermal systems, highlighting the importance of fault pathways and hydrochemical mixing: Example from the Jemez Mountains, New Mexico: Applied Geochemistry, v. 98, p. 45-57, doi.org/10.1016/j.apgeochem.2018.08.015

Michalowsky, T. and Asuero, A.G., 2012, New Approaches in Modeling Carbonate Alkalinity and Total Alkalinity: Critical Reviews in Analytical Chemistry, v. 42(3), p. 220-244.

National Park Service, 2023, Integrated Resource Management Applications: https://irma.nps.gov/Portal.

New Mexico Bureau of Geology and Mineral Resources, 2012, OFGM 132 Valle San Antonio Geodatabase, accessed February 15, 2023 at https://maps.nmt.edu/

Nordstrom, D.K., and Ball., J.W., 1986, The Geochemical Behavior of Aluminum in Acidified Surface Waters: *Science*, v. 232, p. 54-56

Nordstrom, D.K., Ball, J.W., and McCleskey, R.B., 2005, Ground Water to Surface Water: Chemistry of Thermal Outflows in Yellowstone National Park: *Geothermal biology and geochemistry in Yellowstone National Park*, p. 73-94

Nordstrom, D.K., McCleskey, R.B., and Ball, J.W., 2009 Sulfur geochemistry of hydrothermal waters in Yellowstone National Park: IV Acid-sulfate waters: Applied Geochemistry, v. 24, p. 191-207.

Parkhurst, D.L., 1999. User's guide to PHREEQC: a computer program for speciation, reaction path, advective-transport and inverse geochemical calculations: US Geological Survey.

Sherson, L.R., 2012, Nutrient Dynamics in a Headwater Stream: Use of Continuous Water Quality Sensors to Examine Seasonal, Event, and Diurnal Processes in the East Fork Jemez River, NM [M.S. thesis]: University of New Mexico, 92 p.

Smith, J., 2016, CO_2 Flux Along Faults of the Central Rio Grande Rift, New Mexico [M.S. thesis]: University of New Mexico, 115 p.

Smith, R.L., and Bailey, R.A., 1968, Resurgent Cauldrons: Memoir of the Geological Society of America, v. 116, p. 613-662.

Szynkiewicz, A., Johnson, A.P., and Pratt, L.M., 2010, Sulfur species and biosignatures in Sulphur Springs, Valles Caldera, New Mexico—Implications for Mars astrobiology: Earth and Planetary Science Letters, v. 321-322, p. 1-13.

Szynkiewicz, A., Goff, F., Vaniman, D., and Pribil, M.J., 2019, Sulfur cycle in the Valles Caldera volcanic complex, New Mexico, Letter 1: Sulfate sources in aqueous system, and implications for S isotope record on Gale Crater on Mars: Earth and Planetary Science Letters, v. 506, p. 540-551.

U.S. Geological Society, 2022, 3D Elevation Program 1/3 Arc-Second n36w107 20220801, accessed February 14, 2023 at URL https://apps.nationalmap.gov/downloader/

U.S. Geological Survey, 2022, National Hydrography Dataset Best Resolution (NHD) for Hydrological Unit (HU) 8 – 13020201 (published 12092022) Shapefile, accessed February 13, 2023 at URL https://apps.nationalmap.gov/downloader/

Vuataz, F. and Goff, F., 1986, Isotope Geochemistry of Thermal and Nonthermal Waters in the Valles Caldera, Jemez Mountains, Northern New Mexico: Journal of Geophysical Research, v. 91, p. 1835-1853.

Vuataz, F., Goff, F., Fouillac, C., and Calvez, J., 1988, A Strontium Isotope Study of the VC-1 Core Hole and Associated Hydrothermal Fluids and Rocks from Valles Caldera, Jemez Mountains, New Mexico: Journal of Geophysical Research, v. 93, p. 6059-6067.

Wassenaar, L.I., Ahmad, M., Aggarwal, P., van Duren, M., Pöltenstein, L., Araguas, L., and Kurttas, T., 2012, Worldwide proficiency test for routine analysis of δ^2H and $\delta^{18}O$ in water by isotope-ratio mass spectrometry and laser absorption spectroscopy: Rapid Communications in Mass Spectrometry, v. 26(15), p. 1641-1648.

Wilgus, J., Schmandt, B., Maguire, R., Jiang, C., and Chaput, J., 2023, Shear Velocity Evidence of Upper Crustal Magma Storage Beneath Valles Caldera: Geophysical Research Letters, v. 50

List of Tables

Table 1 Modelled low-pH samples

Table 1 Modelled low-pH samples				
	pH measurements			
Sample ID	**Field**	**Model**	**ΔpH**	**T (°C)**
DL21-SC	0.97	2.23	1.26	3.8
DL21-SCBSS	0.17	1.97	1.80	1.9
DL21-SCASS	1.87	2.61	0.74	3.7
DL21-SCARC	2.35	2.93	0.58	4.1
DL21-SCTrib	2.24	2.60	0.36	5.7
DL21-SCASS	2.43	2.89	0.46	3.1
DL22-SCARC	2.60	3.46	0.86	10.9
DL22-SCARC2	1.60	3.04	1.44	6.7
DL22-SCARC	1.61	2.99	1.38	6.7
DL22-SCBFC	2.57	2.95	0.38	8.4
DL22-SCBSS	2.54	2.77	0.23	8.5
DL22-ACASC	2.45	3.07	0.62	11.2
DL23-SCARC	3.20	3.00	0.20	12.8
DL23-SCAFC	2.16	2.82	0.66	10.9
DL23-SCBSS	2.00	2.88	0.88	12.8
DL23-MenBH	1.54	2.30	0.76	48.8
DL23-Lemonade	0.84	1.98	1.14	18.5
DL23-ACASC	2.03	2.84	0.81	14.5
DL23-SCAAC	5.43	10.80	5.37	15.8
DL23-SCBAC	2.22	2.91	0.69	13.2

Table 2

Table 2 Comparisons of low-pH sites measured with a probe vs pH paper

Table 2 Comparisons of low-pH sites measured with a probe and with pH paper				
Name	**Probe T (°C)**	**Thermometer T (°C)**	**pH**	**pH paper**
Tiny Tony Hole	19	19	0.29	0.5
Lemonade	n/a	23.5	0.24	2.5
MBH	54.5	54	0.95	3.2
WBH	53.1	53	0.8	2.8

Table 3a *Table 3 Sample description, collection date, location, and field parameters.*

Table 3a
Sample description, collection date, location, and field parameters

			Field Parameters				
Sample ID		**Sample Date**	**Latitude**	**Longitude**	**T (°C)**	**pH**	**Conductivity (µS/cm)**
Sulphur Creek - Alamo Canyon							
DL21-SCAAC	Sulphur Creek above Alamo Canyon	10/20/2021	35.9229	-106.6008	5.60	5.57	300
DL21-SCAAC	Sulphur Creek above Alamo Canyon	11/10/2021	35.9237	-106.6027	3.50	6.12	312
DL22-SCBAC	Sulphur Creek Below Alamo Canyon	8/3/2022	35.9187	-106.6029	19.20	2.51	1307
DL22-ACASC	Alamo Canyon Above Sulphur Creek	8/3/2022	35.9186	-106.6013	27.30	2.58	1136
DL22-SCAAC	Sulphur Creek above Alamo Canyon	8/3/2022	35.9201	-106.6025	19.90	6.44	258
DL22-SCBAC	Sulphur Creek Below Alamo Canyon	10/12/2022	35.9189	-106.6030	7.00	4.63	283
DL22-ACASC	Alamo Canyon Above Sulphur Creek	10/12/2022	35.9185	-106.6013	11.20	3.08	603
DL22-SCAAC	Sulphur Creek above Alamo Canyon	10/12/2022	35.9198	-106.6025	10.00	5.53	720
DL23-ACASC	Alamo Canyon above Sulphur creek	5/16/2023	35.9187	-106.6027	14.50	2.84	493
DL23-SCBAC	Sulphur Creek below Alamo Canyon	5/16/2023	35.9156	-106.6052	13.20	2.91	342
Sulphur Creek near Sulphur Springs Area							
DL21-SCBSS	Sulphur Creek below Sulphur Springs	10/20/2021	35.9056	-106.6208	1.90	1.97	6000
DL21-SCASS	Sulphur Creek above Sulphur Springs	10/20/2021	35.9127	-106.6081	3.70	2.61	827
DL21-SCASS	Sulphur Creek above Sulphur Springs	11/10/2021	35.9129	-106.6081	3.10	3.06	830
DL22-SCTrib	Sulphur Creek Tributary	1/29/2022	35.8931	-106.6240	0.10	2.83	1620
DL22-SCBSS	Sulphur Creek below Sulphur Springs	8/3/2022	35.9059	-106.6205	21.40	2.36	3320
DL22-SCASS	Sulphur Creek above Sulphur Springs	8/3/2022	35.9129	-106.6081	17.80	2.88	830
DL22-SCBSS	Sulphur Creek below Sulphur Springs	10/12/2022	35.9054	-106.6210	8.50	2.77	1101
DL22-SCASS	Sulphur Creek above Sulphur Springs	10/12/2022	35.9129	-106.6080	7.20	2.97	624
DL23-SCBSS	Sulphur Creek below Sulphur Springs	5/16/2023	35.9036	-106.6213	12.80	2.88	562
Sulphur Creek - Freelove Canyon							
DL21-SC	Sulphur Creek	10/20/2021	35.8970	-106.6236	3.80	2.23	3360
DL21-SCTrib	Sulphur Creek Tributary	11/10/2021	35.8916	-106.6248	5.70	2.76	1884
DL22-SCAFC	Sulphur Creek Above Freelove Canyon	6/14/2022	35.8923	-106.6242	12.40	3.27	1502
DL22-SCBFC	Sulphur Creek Below Freelove Canyon	6/14/2022	35.8905	-106.6245	12.80	5.03	775
DL22-SCBFC	Sulphur Creek Below Freelove Canyon	8/3/2022	35.8906	-106.6244	17.50	2.40	2300
DL22-SCAFC	Sulphur Creek Above Freelove Canyon	8/3/2022	35.8924	-106.6242	16.60	2.40	2840
DL22-FCASC	Freelove Canyon Above Sulphur Creek	8/3/2022	35.8920	-106.6234	14.10	7.31	789
DL22-SCBFC	Sulphur Creek Below Freelove Canyon	10/12/2022	35.8906	-106.6246	8.40	2.95	641
DL22-SCAFC	Sulphur Creek Above Freelove Canyon	10/12/2022	35.8923	-106.6243	7.10	2.75	1227
DL22-FCASC	Freelove Canyon Above Sulphur Creek	10/12/2022	35.8919	-106.6239	10.00	7.61	202
DL23-FCASC	Freelove Canyon above Sulphur Creek	5/16/2023	35.8917	-106.6243	11.20	6.88	202
DL23-SCAFC	Sulphur Creek above Freelove Canyon	5/16/2023	35.8923	-106.6240	10.90	2.82	588
Sulphur Creek - Redondo Creek							
DL21-RCBSC	Redondo Creek Below Sulphur Confluence	11/10/2021	35.8770	-106.6324	3.60	5.41	853
DL21-SCARC	Sulphur Creek Above Redondo Creek	11/10/2021	35.8778	-106.6321	4.10	3.19	890
DL22-SCARC	Sulphur Creek Above Redondo Creek	1/29/2022	35.8778	-106.6321	1.80	3.44	492
DL22-SCARC	Sulphur Creek Above Redondo Creek	6/14/2022	35.8777	-106.6321	10.90	3.46	495
DL22-RCASC	Redondo Creek Above Sulphur Creek	6/14/2022	35.8761	-106.6323	15.90	3.11	659
DL22-RCBSC	Redondo Creek Below Sulphur Creek	6/14/2022	35.8760	-106.6335	16.30	3.36	753
DL22-RCBSC	Redondo Creek Below Sulphur Creek	8/3/2022	35.8760	-106.6332	13.90	2.95	649
DL22-RCASC	Redondo Creek Above Sulphur Creek	8/3/2022	35.8760	-106.6319	13.30	5.35	544
DL22-SCARC	Sulphur Creek Above Redondo Creek	8/3/2022	35.8776	-106.6322	12.10	2.92	973
DL22-RCBSC	Redondo Creek Below Sulphur Creek	10/12/2022	35.8759	-106.6333	5.80	3.29	368
DL22-RCASC	Redondo Creek Above Sulphur Creek	10/12/2022	35.8759	-106.6328	5.00	4.78	148
DL22-SCARC2	Sulphur Creek Above Redondo Creek	10/12/2022	35.8767	-106.6329	6.70	3.04	761
DL22-SCARC	Sulphur Creek Above Redondo Creek	10/12/2022	35.8777	-106.6320	6.70	2.99	773
DL23-RCASC	Redondo Creek above Sulphur Creek	5/16/2023	35.8759	-106.6281	12.50	6.35	126
DL23-RCBSC	Redondo Creek below Sulphur Creek	5/16/2023	35.8761	-106.6335	12.20	4.89	217
DL23-SCARC	Sulphur Creek above Redondo Creek	5/16/2023	35.8776	-106.6318	12.80	3.00	364
Redondo Creek - Rio San Antonio							
DL21-RCASA	Redondo Creek above San Antonio	11/10/2021	35.8661	-106.6390	1.40	5.69	105.9
DL21-SAARC	San Antonio above Redondo Creek Confluence	11/10/2021	35.8662	-106.6395	3.30	6.34	99.8
DL21-SABRC	San Antonio below Redondo Creek Confluence	11/10/2021	35.8657	-106.6390	3.70	7.28	99.5
DL22-RCASA	Redondo Creek above San Antonio	7/8/2022			19.50	5.80	754
DL22-SABRC	San Antonio below Redondo Creek Confluence	8/3/2022	35.8659	-106.6392	16.50	7.46	171
DL22-RCASA	Redondo Creek above San Antonio	8/3/2022	35.8664	-106.6392	14.10	5.77	530
DL22-SAARC	San Antonio above Redondo Creek Confluence	8/3/2022	35.8661	-106.6391	17.20	7.36	163
DL22-SABRC	San Antonio below Redondo Creek Confluence	10/12/2022	35.8656	-106.6387	6.50	5.49	217
DL22-SAARC	San Antonio above Redondo Creek Confluence	10/12/2022	35.8660	-106.6393	6.60	6.89	178
DL22-RCASA	Redondo Creek above San Antonio	10/12/2022	35.8661	-106.6392	5.60	4.10	397
DL23-SABRC	San Antonio Below Redondo Creek Confluence	5/16/2023	35.8653	-106.6387	11.30	6.78	173
DL23-SAARC	San Antonio Above Redondo Creek Confluence	5/16/2023	35.8669	-106.6403	13.40	7.00	157
DL23-RCASA	Redondo Creek above San Antonio Confluence	5/16/2023	35.8666	-106.6389	10.40	5.73	223
Alamo Canyon Geothermal Area							
DL22-ACBWA	Alamo Canyon below white area	7/8/2022	35.9184	-106.6008	26.10	2.18	2570
DL22-ACWA	Alamo Canyon at white area	7/8/2022	35.9180	-106.6002	20.90	2.76	729
DL22-ACAWA	Alamo Canyon above white area	7/8/2022	35.9176	-106.5971	25.30	2.70	765
Sulphur Springs Area							
DL22-MenBH	Men's Bathhouse Spring	7/8/2022	35.9068	-106.6161	61.70	2.13	5130
DL22-WomenBH	Women's Bathhouse Spring	7/8/2022	35.9062	-106.6164	32.40	1.64	12480
DL22-Lemonade	Lemonade Spring	7/8/2022	35.9062	-106.6164	60.50	2.11	3810
DL23-MenBH	Men's Bathhouse Mudpot	5/16/2023	35.9069	-106.6160	48.80	1.54	2940
DL23-Lemonade	Lemonade Spring	5/16/2023	35.9073	-106.6162	18.50	1.98	6290

Table 3b

Table 3b

Major ion compositions and calculated TDS values

			Major Ion Concentrations [mg/kg]						
Sample ID		**Sample Date**	**Ca**	**Mg**	**Na**	**K**	**HCO3**	**Cl**	**SO4**
Sulphur Creek - Alamo Canyon									
DL21-SCAAC	Sulphur Creek above Alamo Canyon	10/20/2021	22.07	3.22	19.86	16.26	17.51	3.31	101.32
DL21-SCAAC	Sulphur Creek above Alamo Canyon	11/10/2021	20.88	2.91	18.75	12.31	21.97	3.14	93.94
DL22-SCBAC	Sulphur Creek Below Alamo Canyon	8/3/2022	37.54	6.07	13.64	14.54	0.00	3.27	437.04
DL22-ACASC	Alamo Canyon Above Sulphur Creek	8/3/2022	38.38	6.99	14.75	14.27	0.00	3.71	398.69
DL22-SCAAC	Sulphur Creek above Alamo Canyon	8/3/2022	24.74	3.56	17.20	11.55	76.27	1.74	56.82
DL22-SCBAC	Sulphur Creek Below Alamo Canyon	10/12/2022	28.76	4.39	12.77	10.24	14.64	13.79	101.89
DL22-ACASC	Alamo Canyon Above Sulphur Creek	10/12/2022	20.56	3.81	8.74	9.51	0.00	13.22	187.11
DL22-SCAAC	Sulphur Creek above Alamo Canyon	10/12/2022	27.84	4.21	11.52	9.64	22.58	2.17	92.48
DL23-ACASC	Alamo Canyon above Sulphur creek	5/16/2023	11.62	1.94	6.22	4.22	0.00	3.51	153.18
DL23-SCBAC	Sulphur Creek below Alamo Canyon	5/16/2023	13.99	2.21	6.03	4.32	0.00	3.60	144.53
Sulphur Creek near Sulphur Springs Area									
DL21-SCBSS	Sulphur Creek below Sulphur Springs	10/20/2021	142.70	25.66	19.82	34.02	0.00	21.09	2025.71
DL21-SCASS	Sulphur Creek above Sulphur Springs	10/20/2021	45.73	5.80	19.00	12.35	0.00	3.26	368.12
DL21-SCASS	Sulphur Creek above Sulphur Springs	11/10/2021	48.89	7.29	21.23	16.75	0.00	3.53	378.37
DL22-SCTrib	Sulphur Creek Tributary	1/29/2022	131.60	19.59	25.12	20.90	0.00	6.21	1313.74
DL22-SCBSS	Sulphur Creek below Sulphur Springs	8/3/2022	104.10	20.23	19.90	28.89	0.00	2.21	1341.07
DL22-SCASS	Sulphur Creek above Sulphur Springs	8/3/2022	45.95	6.96	16.42	16.15	0.00	2.60	381.73
DL22-SCBSS	Sulphur Creek below Sulphur Springs	10/12/2022	39.40	6.58	10.93	12.56	0.00	12.26	351.60
DL22-SCASS	Sulphur Creek above Sulphur Springs	10/12/2022	24.60	4.44	9.84	11.26	0.00	14.04	238.53
DL23-SCBSS	Sulphur Creek below Sulphur Springs	5/16/2023	25.21	3.38	6.75	5.92	0.00	3.46	211.97
Sulphur Creek - Freelove Canyon									
DL21-SC	Sulphur Creek	10/20/2021	119.00	17.72	22.98	24.01	0.00	22.36	1334.54
DL21-SCTrib	Sulphur Creek Tributary	11/10/2021	117.80	18.34	27.71	20.67	0.00	4.26	1008.56
DL22-SCAFC	Sulphur Creek Above Freelove Canyon	6/14/2022	105.20	16.92	26.18	18.89	0.00	4.41	888.73
DL22-SCBFC	Sulphur Creek Below Freelove Canyon	6/14/2022	92.46	13.88	40.81	15.24	0.00	8.36	351.60
DL22-SCBFC	Sulphur Creek Below Freelove Canyon	8/3/2022	96.04	18.80	25.55	24.28	0.00	4.44	1100.00
DL22-SCAFC	Sulphur Creek Above Freelove Canyon	8/3/2022	100.40	19.93	22.16	26.83	0.00	5.32	1486.38
DL22-FCASC	Freelove Canyon Above Sulphur Creek	8/3/2022	77.11	12.97	70.66	12.65	388.07	7.00	110.97
DL22-SCBFC	Sulphur Creek Below Freelove Canyon	10/12/2022	33.96	5.82	17.42	11.85	0.00	13.72	279.83
DL22-SCAFC	Sulphur Creek Above Freelove Canyon	10/12/2022	42.84	7.22	11.79	13.51	0.00	13.67	396.14
DL22-FCASC	Freelove Canyon Above Sulphur Creek	10/12/2022	17.34	2.94	23.10	4.04	79.32	3.02	32.72
DL23-FCASC	Freelove Canyon above Sulphur Creek	5/16/2023	17.27	2.85	17.50	3.01	59.80	3.22	32.89
DL23-SCAFC	Sulphur Creek above Freelove Canyon	5/16/2023	21.75	3.50	7.08	6.20	0.00	3.71	215.41
Sulphur Creek - Redondo Creek									
DL21-RCBSC	Redondo Creek Below Sulphur Confluence	11/10/2021	79.43	10.58	34.04	14.16	0.00	32.72	536.84
DL21-SCARC	Sulphur Creek Above Redondo Creek	11/10/2021	81.52	12.07	28.68	13.42	0.00	6.73	443.58
DL22-SCARC	Sulphur Creek Above Redondo Creek	1/29/2022	80.12	10.81	31.47	12.82	0.00	16.17	394.88
DL22-SCARC	Sulphur Creek Above Redondo Creek	6/14/2022	98.44	13.82	33.10	13.67	0.00	6.88	546.98
DL22-RCASC	Redondo Creek Above Sulphur Creek	6/14/2022	69.73	9.68	33.13	13.33	0.00	28.34	353.78
DL22-RCBSC	Redondo Creek Below Sulphur Creek	6/14/2022	78.72	11.09	33.95	12.78	0.00	18.18	391.48
DL22-RCBSC	Redondo Creek Below Sulphur Creek	8/3/2022	64.02	9.85	30.12	15.96	0.00	22.73	340.21
DL22-RCASC	Redondo Creek Above Sulphur Creek	8/3/2022	58.70	8.41	27.67	15.19	0.00	22.90	297.96
DL22-SCARC	Sulphur Creek Above Redondo Creek	8/3/2022	80.41	10.99	28.42	14.30	0.00	7.35	490.87
DL22-RCBSC	Redondo Creek Below Sulphur Creek	10/12/2022	32.29	4.78	16.21	8.73	0.00	13.82	157.16
DL22-RCASC	Redondo Creek Above Sulphur Creek	10/12/2022	15.55	2.05	9.00	3.37	45.15	12.90	10.74
DL22-SCARC2	Sulphur Creek Above Redondo Creek	10/12/2022	47.62	7.32	21.59	13.90	0.00	22.59	304.28
DL22-SCARC	Sulphur Creek Above Redondo Creek	10/12/2022	46.33	6.97	20.75	13.45	0.00	14.83	304.94
DL23-RCASC	Redondo Creek above Sulphur Creek	5/16/2023	10.25	1.51	7.00	2.39	36.61	4.83	9.38
DL23-RCBSC	Redondo Creek below Sulphur Creek	5/16/2023	19.55	2.55	9.61	3.96	6.10	6.30	77.07
DL23-SCARC	Sulphur Creek above Redondo Creek	5/16/2023	24.33	4.40	13.48	6.48	0.00	5.44	191.90
Redondo Creek - Rio San Antonio									
DL21-RCASA	Redondo Creek above San Antonio	11/10/2021	9.93	1.28	15.01	2.43	59.19	3.17	8.15
DL21-SAARC	San Antonio above Redondo Creek Confluence	11/10/2021	9.84	1.25	14.98	2.25	58.58	2.89	8.06
DL21-SABRC	San Antonio below Redondo Creek Confluence	11/10/2021	9.82	1.25	14.78	2.27	60.41	2.73	8.07
DL22-RCASA	Redondo Creek above San Antonio	7/8/2022	57.20	8.77	48.64	11.86	57.36	64.12	153.44
DL22-SABRC	San Antonio below Redondo Creek Confluence	8/3/2022	15.18	2.18	13.44	3.55	71.39	1.75	8.79
DL22-RCASA	Redondo Creek above San Antonio	8/3/2022	48.19	6.87	37.20	10.62	62.85	45.78	147.73
DL22-SAARC	San Antonio above Redondo Creek Confluence	8/3/2022	14.88	2.17	13.33	3.83	76.88	1.86	8.79
DL22-SABRC	San Antonio below Redondo Creek Confluence	10/12/2022	20.41	3.24	14.44	4.62	56.14	15.52	38.21
DL22-SAARC	San Antonio above Redondo Creek Confluence	10/12/2022	17.81	2.78	15.68	3.58	76.88	4.04	9.77
DL22-RCASA	Redondo Creek above San Antonio	10/12/2022	34.69	5.06	17.30	9.08	0.00	19.06	160.04
DL23-SABRC	San Antonio Below Redondo Creek Confluence	5/16/2023	15.26	2.81	11.44	3.26	44.30	4.83	30.83
DL23-SAARC	San Antonio Above Redondo Creek Confluence	5/16/2023	14.39	2.77	11.60	2.75	59.80	4.22	8.30
DL23-RCASA	Redondo Creek above San Antonio Confluence	5/16/2023	20.01	2.90	10.72	4.28	8.54	6.00	67.58
Alamo Canyon Geothermal Area									
DL22-ACBWA	Alamo Canyon below white area	7/8/2022	59.10	9.37	21.06	17.46	0.00	4.04	829.47
DL22-ACWA	Alamo Canyon at white area	7/8/2022	50.35	8.08	18.34	12.55	0.00	6.55	327.46
DL22-ACAWA	Alamo Canyon above white area	7/8/2022	56.21	8.70	17.67	13.21	0.00	4.43	361.99
Sulphur Springs Area									
DL22-MenBH	Men's Bathhouse Spring	7/8/2022	444.80	22.09	41.96	55.78	0.00	13.45	4837.27
DL22-WomenBH	Women's Bathhouse Spring	7/8/2022	290.60	66.98	134.60	234.90	0.00	34.11	11851.84
DL22-Lemonade	Lemonade Spring	7/8/2022	155.10	41.82	7.21	7.27	0.00	4.46	1989.93
DL23-MenBH	Men's Bathhouse Mudpot	5/16/2023	154.70	15.38	18.40	13.58	0.00	3.11	982.59
DL23-Lemonade	Lemonade Spring	5/16/2023	260.00	68.99	16.35	18.81	0.00	5.47	2735.41

Table 3c

Table 3c

Trace ions, stable water isotopes, and Sr isotopes

			Trace Ions				Stable Isotopes (‰)		Radiogenic Isotopes	
Sample ID		**Sample Date**	**Al**	**Fe**	**Mn**	**Si**	**$\delta^{18}O$**	**δD**	**Sr [mg/kg]**	**$^{87}Sr/^{86}Sr$**
Sulphur Creek - Alamo Canyon										
DL21-SCAAC	Sulphur Creek above Alamo Canyon	10/20/2021	NA	1.27	0.00	34.39	-12.1722	-86.3020		
DL21-SCAAC	Sulphur Creek above Alamo Canyon	11/10/2021	NA	NA	0.00	35.72	-12.2935	-86.7090		
DL22-SCBAC	Sulphur Creek Below Alamo Canyon	8/3/2022	13.55	8.94	0.00	32.90	-7.5583	-53.9410		
DL22-ACASC	Alamo Canyon Above Sulphur Creek	8/3/2022	10.14	5.34	1.11	26.39	-6.9336	-50.9697		
DL22-SCAAC	Sulphur Creek above Alamo Canyon	8/3/2022	NA	0.78	0.00	19.88	-8.2598	-55.7653		
DL22-SCBAC	Sulphur Creek Below Alamo Canyon	10/12/2022	NA	0.24	0.00	17.69	-9.7118	-65.1281		
DL22-ACASC	Alamo Canyon Above Sulphur Creek	10/12/2022	10.76	3.63	0.00	27.35	-10.3371	-70.2047		
DL22-SCAAC	Sulphur Creek above Alamo Canyon	10/12/2022	NA	NA	0.00	19.11	-9.7760	-65.5411		
DL23-ACASC	Alamo Canyon above Sulphur creek	5/16/2023	3.71	2.24		22.50	-11.8001	-82.4412		
DL23-SCBAC	Sulphur Creek below Alamo Canyon	5/16/2023	4.16	1.52		20.87	-11.4691	-81.1589		
Sulphur Creek near Sulphur Springs Area										
DL21-SCBSS	Sulphur Creek below Sulphur Springs	10/20/2021	116.60	59.92	0.00	52.68	-11.0680	-71.8364		
DL21-SCASS	Sulphur Creek above Sulphur Springs	10/20/2021	17.13	1.93	1.14	34.87	-10.8684	-77.1948		
DL21-SCASS	Sulphur Creek above Sulphur Springs	11/10/2021	16.89	1.77	1.06	36.27	-11.0105	-76.9861		
DL22-SCTrib	Sulphur Creek Tributary	1/29/2022	101.60	24.24	2.52	50.17	-11.0500	-74.2000		
DL22-SCBSS	Sulphur Creek below Sulphur Springs	8/3/2022	63.98	38.40	2.76	45.74	-10.0147	-67.0050		
DL22-SCASS	Sulphur Creek above Sulphur Springs	8/3/2022	20.74	4.29	1.20	36.48	-10.2987	-70.7203		
DL22-SCBSS	Sulphur Creek below Sulphur Springs	10/12/2022	20.64	8.21	0.00	30.25	-9.7655	-66.3197		
DL22-SCASS	Sulphur Creek above Sulphur Springs	10/12/2022	11.94	4.50	0.00	27.83	-10.1461	-68.5435		
DL23-SCBSS	Sulphur Creek below Sulphur Springs	5/16/2023	7.76	3.16		22.61	-11.4993	-81.4208		
Sulphur Creek - Freelove Canyon										
DL21-SC	Sulphur Creek	10/20/2021	89.69	40.37	2.21	53.89	-10.4642	-71.0418		
DL21-SCTrib	Sulphur Creek Tributary	11/10/2021	70.25	15.94	2.29	52.69	-10.4976	-72.0673		
DL22-SCAFC	Sulphur Creek Above Freelove Canyon	6/14/2022	54.75	11.17	2.07	49.14	-11.2993	-78.9480		
DL22-SCBFC	Sulphur Creek Below Freelove Canyon	6/14/2022	1.76	10.78	1.68	27.51	-11.4751	-80.7699		
DL22-SCBFC	Sulphur Creek Below Freelove Canyon	8/3/2022	69.36	29.93	2.34	50.91	-9.8054	-66.6083	0.471313	0.708824
DL22-SCAFC	Sulphur Creek Above Freelove Canyon	8/3/2022	83.00	37.06	2.54	56.14	-9.6199	-64.5732	0.457438	0.708983
DL22-FCASC	Freelove Canyon Above Sulphur Creek	8/3/2022	NA	NA	0.00	20.22	-11.1425	-77.3044	0.658665	0.708040
DL22-SCBFC	Sulphur Creek Below Freelove Canyon	10/12/2022	12.73	4.87	0.00	26.76	-10.3402	-69.9906		
DL22-SCAFC	Sulphur Creek Above Freelove Canyon	10/12/2022	22.11	7.96	0.00	32.80	-9.8019	-65.5394		
DL22-FCASC	Freelove Canyon Above Sulphur Creek	10/12/2022	NA	NA	0.00	17.87	-11.2720	-78.3579		
DL23-FCASC	Freelove Canyon above Sulphur Creek	5/16/2023	NA	NA		16.79	-12.1676	-84.7418		
DL23-SCAFC	Sulphur Creek above Freelove Canyon	5/16/2023	7.93	2.66		23.40	-11.5343	-81.3343		
Sulphur Creek - Redondo Creek										
DL21-RCBSC	*Redondo Creek Below Sulphur Confluence*	*11/10/2021*	*5.81*	*2.67*	*2.34*	*25.31*	*-11.0470*	*-77.9010*		
DL21-SCARC	Sulphur Creek Above Redondo Creek	11/10/2021	8.65	6.45	2.67	25.40	-11.2252	-77.8274		
DL22-SCARC	Sulphur Creek Above Redondo Creek	1/29/2022	3.94	7.16	2.26	22.75	-11.2200	-78.5000		
DL22-SCARC	Sulphur Creek Above Redondo Creek	6/14/2022	16.53	4.70	3.31	29.36	-11.5572	-80.8641		
DL22-RCASC	Redondo Creek Above Sulphur Creek	6/14/2022	8.87	1.46	1.87	31.49	-11.5334	-80.9551		
DL22-RCBSC	Redondo Creek Below Sulphur Creek	6/14/2022	7.93	1.37	2.33	29.35	-11.3821	-80.0976		
DL22-RCBSC	Redondo Creek Below Sulphur Creek	8/3/2022	5.25	2.10	2.15	26.88	-11.1973	-77.9421		
DL22-RCASC	Redondo Creek Above Sulphur Creek	8/3/2022	7.31	1.62	1.67	29.41	-11.4681	-80.3170		
DL22-SCARC	Sulphur Creek Above Redondo Creek	8/3/2022	11.65	6.74	2.92	25.24	-11.1812	-77.9363		
DL22-RCBSC	Redondo Creek Below Sulphur Creek	10/12/2022	6.07	0.68	0.00	22.11	-10.5427	-71.7835		
DL22-RCASC	Redondo Creek Above Sulphur Creek	10/12/2022	NA	0.30	0.00	17.56	-10.9488	-74.5867		
DL22-SCARC2	Sulphur Creek Above Redondo Creek	10/12/2022	13.15	4.06	1.26	28.10	-10.1910	-69.1703		
DL22-SCARC	Sulphur Creek Above Redondo Creek	10/12/2022	12.54	4.21	1.24	27.31	-10.1828	-69.4576		
DL23-RCASC	Redondo Creek above Sulphur Creek	5/16/2023	NA	0.12		13.69	-11.9052	-82.8251		
DL23-RCBSC	Redondo Creek below Sulphur Creek	5/16/2023	NA	0.30		17.35	-11.7777	-82.3931		
DL23-SCARC	Sulphur Creek above Redondo Creek	5/16/2023	5.16	1.88		22.66	-11.6141	-81.8891		
Redondo Creek - Rio San Antonio										
DL21-RCASA	Redondo Creek above San Antonio	11/10/2021	NA	NA	0.00	29.95	-12.0592	-86.8716		
DL21-SAARC	San Antonio above Redondo Creek Confluence	11/10/2021	NA	NA	0.00	30.44	-12.2230	-86.5184		
DL21-SABRC	San Antonio below Redondo Creek Confluence	11/10/2021	NA	NA	0.00	30.64	-12.2805	-86.7960		
DL22-RCASA	Redondo Creek above San Antonio	7/8/2022	0.22	NA	1.52	75.02	-10.3424	-72.7043	0.277107	0.708718
DL22-SABRC	San Antonio below Redondo Creek Confluence	8/3/2022	NA	0.28	0.00	27.58	-10.0800	-69.9183		
DL22-RCASA	Redondo Creek above San Antonio	8/3/2022	NA	1.85	1.01	16.94	-8.8255	-58.8032		
DL22-SAARC	San Antonio above Redondo Creek Confluence	8/3/2022	NA	0.30	0.00	26.29	-10.1492	-69.6917		
DL22-SABRC	San Antonio below Redondo Creek Confluence	10/12/2022	0.56	0.11	0.00	24.29	-10.7918	-74.4810		
DL22-SAARC	San Antonio above Redondo Creek Confluence	10/12/2022	NA	0.14	0.00	26.07	-10.9794	-75.4872		
DL22-RCASA	Redondo Creek above San Antonio	10/12/2022	5.20	0.20	0.00	21.94	-10.4917	-71.2993		
DL23-SABRC	San Antonio Below Redondo Creek Confluence	5/16/2023	NA	NA		18.55	-11.9609	-84.1709		
DL23-SAARC	San Antonio Above Redondo Creek Confluence	5/16/2023	NA	NA		16.75	-11.9749	-84.9315		
DL23-RCASA	Redondo Creek above San Antonio Confluence	5/16/2023	NA	0.12		16.11	-11.7606	-82.4715		
Alamo Canyon Geothermal Area										
DL22-ACBWA	Alamo Canyon below white area	7/8/2022	22.88	12.84	1.13	86.23	-9.4480	-67.5296		
DL22-ACWA	Alamo Canyon at white area	7/8/2022	5.17	6.53	1.06	81.18	-9.8697	-69.1864	0.342594	0.707688
DL22-ACAWA	Alamo Canyon above white area	7/8/2022	3.96	15.19	1.34	82.32	-7.1324	-55.9295		
Sulphur Springs Area										
DL22-MenBH	Men's Bathhouse Spring	7/8/2022	250.60	123.00	1.96	225.30	-1.3371	-40.4796	1.813950	0.708338
DL22-WomenBH	Women's Bathhouse Spring	7/8/2022	873.70	155.20	3.41	139.60	-14.9719	-79.9762	1.720948	0.711106
DL22-Lemonade	Lemonade Spring	7/8/2022	62.49	29.86	2.66	161.50	-11.4321	-66.6580	0.041664	0.711529
DL23-MenBH	Men's Bathhouse Mudpot	5/16/2023	20.42	17.16		83.81	-5.8113	-58.2980		
DL23-Lemonade	Lemonade Spring	5/16/2023	137.30	82.82	4.98	105.30	-10.2029	-67.1433		

Table 4

Table 4 Sr-isotope analysis results

Table 4 Sr-isotope analysis results				
	Sr-concentration (ppm)			
Sample ID	**ICP-OES**	**ICP-MS**	**$^{87}Sr/^{86}Sr$**	**2σ**
DL22-MenBH	1.9	1.81	0.708338	3.28659E-05
DL22-WomenBH	1.8	1.72	0.711106	2.10481E-05
DL22-Lemonade	0.0	0.04	0.711529	3.49196E-05
DL22-ACWA	0.3	0.34	0.707688	2.20791E-05
DL22-RCASA	0.3	0.28	0.708718	0.00002
DL22-SCBFC	0.6	0.47	0.708824	0.00002
DL22-SCAFC	0.5	0.46	0.708983	2.5239E-05
DL22-FCASC	0.7	0.66	0.708040	0.00002

Table 5 *Table 5 Saturation indices for selected minerals and samples in the Sulphur Creek field area*

Table 5
Saturation Indices for selected minerals and samples in the Sulphur Creek field area

			Saturation Indices								
Sample ID	Season	pH	Al(OH)3 (am)	SiO2 (am)	Gibbsite	Alunite	Jarosite-K	Kaolinite	Goethite	Illite	Hematite
Sulphur Creek - Alamo Canyon											
DL21-SCAAC	Fall/Winter	5.57	--	-0.03	--	--	-11.55	--	2.66	--	7.23
DL21-SCAAC	Fall/Winter	6.12	--	0.01	--	--	--	--	--	--	--
DL22-SCAAC	Spring/Summer	6.44	--	-0.40	--	--	--	--	--	--	--
DL22-SCAAC	Fall/Winter	5.53	--	-0.33	--	--	--	--	--	--	--
DL22-ACASC	Fall/Winter	3.08	-6.63	-0.18	-3.81	-3.84	-24.21	-4.49	-4.02	-11.99	-6.11
DL23-ACASC	Spring/Summer	2.84	-7.55	-0.29	-4.76	-6.57	-26.13	-6.65	-4.72	-15.09	-7.48
DL22-SCBAC	Fall/Winter	4.63	--	-0.33	--	--	--	--	--	--	--
DL23-SCBAC	Spring/Summer	2.91	-7.34	-0.32	-4.53	-6.10	--	-6.23	--	-14.54	--
Sulphur Creek Above/Below Sulphur Springs Area											
DL21-SCASS	Fall/Winter	3.06	-7.77	0.02	-4.87	-5.29	-27.06	-6.13	-5.50	-13.80	-9.10
DL22-SCASS	Spring/Summer	2.88	-6.69	-0.11	-3.94	-3.27	-23.65	-4.67	-4.19	-12.04	-6.40
DL22-SCASS	Fall/Winter	2.97	-7.25	-0.14	-4.39	-4.80	-25.01	-5.52	-4.53	-13.25	-7.13
DL21-SCBSS	Fall/Winter	1.97	-10.20	0.20	-7.28	-8.60	-27.58	-10.59	-6.98	-19.50	-12.06
DL22-SCTrib	Fall/Winter	2.83	-7.74	0.19	-4.80	-3.96	-24.08	-5.62	-4.87	-13.03	-7.86
DL22-SCBSS	Spring/Summer	2.36	-7.89	-0.04	-5.17	-4.65	-22.89	-7.03	-4.72	-14.96	-7.46
DL23-SCBSS	Spring/Summer	2.00	-7.29	-0.28	-4.48	-5.45	-25.42	-6.05	-4.57	-14.22	-7.20
Sulphur Creek - Freelove Canyon											
DL21-SC	Fall/Winter	2.23	-9.30	0.19	-6.40	-7.16	-26.41	-8.86	-6.19	-17.31	-10.49
DL21-SCTrib	Fall/Winter	2.76	-8.08	0.16	-5.20	-4.98	-25.17	-6.54	-5.32	-14.25	-8.73
DL22-SCAFC	Spring/Summer	3.27	-5.73	0.07	-2.92	-0.50	-20.57	-2.22	-3.03	-8.57	-4.12
DL22-SCAFC	Spring/Summer	2.40	-7.95	0.09	-5.18	-4.63	-23.44	-6.75	-4.90	-14.54	-7.84
DL22-SCAFC	Fall/Winter	2.75	-7.78	-0.06	-4.92	-5.35	-25.37	-6.43	-4.99	-14.38	-8.06
DL23-SCAFC	Spring/Summer	2.82	-7.59	-0.25	-4.76	-5.99	-26.27	-6.52	-4.94	-14.81	-7.95
DL22-FCASC	Fall/Winter	7.61	--	-0.36	--	--	--	--	--	--	--
DL23-FCASC	Spring/Summer	6.88	--	-0.39	--	--	--	--	--	--	--
DL22-SCBFC	Spring/Summer	5.03	-1.70	-0.19	1.10	5.64	-10.34	5.30	2.34	1.67	6.64
DL22-SCBFC	Spring/Summer	2.40	-7.92	0.04	-5.16	-4.75	-23.66	-6.81	-4.92	-14.68	-7.87
DL22-SCBFC	Fall/Winter	2.95	-7.24	-0.16	-4.39	-4.67	-24.70	-5.60	-4.48	-13.33	-7.03
Sulphur Creek - Redondo Creek											
DL21-SCARC	Fall/Winter	3.19	-7.91	-0.15	-5.02	-5.91	-24.95	-6.77	-4.75	-14.67	-7.60
DL22-SCARC	Spring/Summer	3.46	-5.61	-0.15	-2.78	-1.08	-21.08	-2.36	-2.87	-8.88	-3.80
DL22-SCARC	Fall/Winter	2.99	-7.29	-0.14	-4.42	-4.66	-24.88	-5.58	-4.56	-13.23	-7.20
DL23-SCARC	Spring/Summer	3.00	-7.10	-0.28	-4.29	-5.24	-25.39	-5.67	-4.44	-13.59	-6.93
DL22-RCASC	Spring/Summer	5.35	-0.11	-0.17	2.69	9.34	-10.84	8.52	2.53	5.72	7.02
DL22-RCASC	Fall/Winter	4.78	--	-0.31	--	--	--	--	--	--	--
DL23-RCASC	Spring/Summer	6.35	--	-0.49	--	--	--	--	--	--	--
DL21-RCBSC	Fall/Winter	5.41	-0.72	-0.14	2.18	8.26	-11.33	7.64	2.27	4.62	6.44
DL22-RCBSC	Spring/Summer	2.95	-7.33	-0.21	-4.54	-5.11	-24.77	-6.03	-4.53	-13.67	-7.10
DL22-RCBSC	Fall/Winter	3.29	-6.58	-0.22	-3.70	-4.02	--	-4.30	--	-11.68	--
DL23-RCBSC	Spring/Summer	4.89	--	-0.39	--	--	--	--	--	--	--
Redondo Creek - Rio San Antonio											
DL21-RCASA	Fall/Winter	5.69	--	-0.05	--	--	--	--	--	--	--
DL22-RCASA	Spring/Summer	5.80	--	0.19	--	--	--	--	--	--	--
DL22-RCASA	Spring/Summer	5.77	--	-0.41	--	--	-8.66	--	3.91	--	9.78
DL22-RCASA	Fall/Winter	4.10	-4.25	-0.22	-1.37	0.62	--	0.36	--	-5.42	--
DL21-SAARC	Fall/Winter	6.34	--	-0.06	--	--	--	--	--	--	--
DL22-SAARC	Spring/Summer	7.36	--	-0.25	--	--	--	--	--	--	--
DL21-SABRC	Fall/Winter	7.28	--	-0.06	--	--	--	--	--	--	--
DL22-SABRC	Spring/Summer	7.46	--	-0.23	--	--	--	--	--	--	--
Alamo Canyon Geothermal Areas											
DL22-ACAWA	Spring/Summer	2.70	-7.48	0.18	-4.80	-5.76	-22.08	-5.88	-3.73	-13.19	-5.46
DL22-ACWA	Spring/Summer	2.76	-7.44	0.21	-4.71	-5.54	-23.50	-5.60	-4.17	-12.85	-6.35
DL22-ACBWA	Spring/Summer	2.18	-8.43	0.19	-5.75	-6.59	-25.05	-7.77	-5.40	-15.85	-8.80
Sulphur Springs Vents											
DL22-MenBH	Spring/Summer	2.13	-6.07	0.36	-3.68	-0.49	-17.55	-3.57	-3.02	-10.26	-3.89
DL23-MenBH	Spring/Summer	1.54	-6.85	0.01	-4.37	-3.86	-21.13	-5.55	-3.72	-13.16	-5.33
DL23-Lemonade	Spring/Summer	1.98	-9.05	0.35	-6.30	-6.69	-24.78	-8.48	-5.79	-16.64	-9.61
DL22-WomenBH	Spring/Summer	1.64	-8.77	0.37	-6.14	-4.27	-23.12	-8.24	-5.95	-15.95	-9.87
DL22-Lemonade	Spring/Summer	2.11	-6.47	0.22	-4.07	-2.94	-20.53	-4.63	-3.58	-12.06	-5.01

Table 6

Table 6 CO_2 flux results from selected Sulphur Springs vents; modified from Smith (2019)

Table 6 CO_2 flux results from selected Sulphur Springs vents; modified from Smith (2019)					
			CO_2 Flux		
Location	**Latitude**	**Longitude**	**g/m^2 /hr**	**g/m^2 /day**	**mol/m^2 /d**
Sulphur Springs - Men's Bathhouse	35.906900	106.616150	3357.9*	80591.8*	1827.5*
Sulphur Springs - Women's Bathhouse (KK)	35.906467	106.616367	100	2399.8	54.42
Sulphur Springs - Lemon Spring (KK)	35.907333	106.616150	100	2399.8	54.42
Sulphur Springs - Footbath Spring (KK)	35.908017	106.615650	7088.1*	170115.8*	3857.5*

* Flux calculated by hand, see Smith (2019) methods section

KK = Karl Karlstrom Array

Table 7

Table 7 Discharge data for selected gauges

Table 7 Discharge data for selected gauges				
		Sulphur Creek HOBO's		**Jemez River**
		Upper	**Lower**	**USGS Gauge 08324000**
	Earliest Record	5/24/2013	5/27/2013	5/24/2013
	Maximum Discharge	21.10	39.66	1100.00
	Date of Maximum Discharge	4/9/2023	4/13/2023	4/13/2023
	Minimum Discharge	0.00	0.00	3.04
	Date of Minimum Discharge	9/28/2014	9/23/2017	7/13/2020
Flow Percentiles (cfs)	100%	21.10	39.66	1100.00
	75%	0.33	0.75	41.20
	50%	0.25	0.36	22.20
	25%	0.15	0.16	15.40
	0%	0.00	0.00	3.04

Table 8

Table 8 Estimated mass-loading calculations for Sulphur Creek

Table 8
Estimated loading calculations for Sulphur Creek

				Concentration [mg/kg]					Load [mg/s]			
Sample ID	**Sample Site**	**Sample Date**	**Season**	**Al**	**Fe**	**SO4**	**Discharge (cfs)***	**Discharge (L/s)**	**Al**	**Fe**	**SO4**	
Stand-Alone Load Values												
DL21-SCAAC	SCAAC	10/20/2021	FW	NA	1.3	101.3	0.3	8.0	NA	10.1	807.7	
11/10/2021 Estimated Load												
DL21-SCAAC	SCAAC	11/10/2021	FW	NA	NA	93.9	0.4	9.9	NA	NA	932.5	Upstream
*RSA Battleship***	*SABRC*	*8/25/2018*	*SS*	*0.0*	*--*	*7.1*	*3.8*	*107.9*	*2.3*	*NA*	*760.6*	Downstream
8/3/2022 Estimated Load												
DL22-SCAAC	SCAAC	8/3/2022	SS	NA	0.8	56.8	0.3	7.7	NA	6.0	436.7	Upstream
DL22-SCBAC	SCBAC	8/3/2022	SS	13.6	8.9	437.0	0.7	18.8	254.4	167.8	8205.4	
*RSA Battleship****	*SABRC*	*10/25/2006*	*FW*	*--*	*--*	*16.2*	*9.5*	*269.0*	*NA*	*NA*	*4358.0*	Downstream
10/12/2022 Estimated Load												
DL22-SCAAC	SCAAC	10/12/2022	FW	NA	NA	92.5	0.3	9.2	NA	NA	849.1	Upstream
DL22-SCBAC	SCBAC	10/12/2022	FW	NA	NA	101.9	2.0	56.8	NA	NA	5791.1	
DL22-SCBSS	SCBSS	10/12/2022	FW	19.7	8.2	369.3	0.7	19.8	391.3	162.9	7324.1	Downstream
5/16/2023 Estimated Load												
DL23-SCAAC	SCAAC	5/16/2023	SS	NA	2.4	25.1	0.8	22.8	NA	53.7	571.3	Upstream
DL23-SCBAC	SCBAC	5/16/2023	SS	4.2	1.5	144.5	2.7	76.9	320.4	116.8	11121.1	Downstream
Yellowstone Comparisons - McCleskey et al. (2010a, 2010b)												
Sample ID	**Sample Site**	**Sample Date**	**Season**	**Al**	**Fe**	**SO4**	**Discharge (m^3/s)******	**Discharge (L/s)**	**Al**	**Fe**	**SO4**	
Gibbon River at NPS Museum	G2	9/12/2006	FW	0.04	NA	6.6	1.3	1290.0	50.3	NA	8462.4	Upstream
Gibbon River Upstream from Flook Ck	G4	9/13/2006	FW	0.34	0.26	26.4	1.5	1450.0	491.6	381.4	38280.0	
Gibbon River at Elk Park	G7	9/13/2006	FW	0.23	0.31	28.7	1.4	1410.0	320.1	439.9	40467.0	Downstream

*Sulphur Creek discharges have measurement errors of ±5%

**SO_4 load estimated from Golla (2019) based on similar daily mean discharge at USGS Jemez Gauge

***SO_4 load estimated from Dyer (2007) based on similar daily mean discharge at USGS Jemez Gauge

****Gibbon River discharges have measurement errors of up to ±10%

SCAAC = Sulphur Creek Above Alamo Canyon

SCBAC = Sulphur Creek Below Alamo Canyon

SCBSS = Sulphur Creek Below Sulphur Springs

FW = Fall/Winter

SS = Spring/Summer

SCAAC Discharges taken from Upper Sulphur HOBO

SCBAC Discharges taken from Lower Sulphur HOBO

SCBSS Discharges taken from Sulphur Creek Flume (where available)

Figures

Figure 1

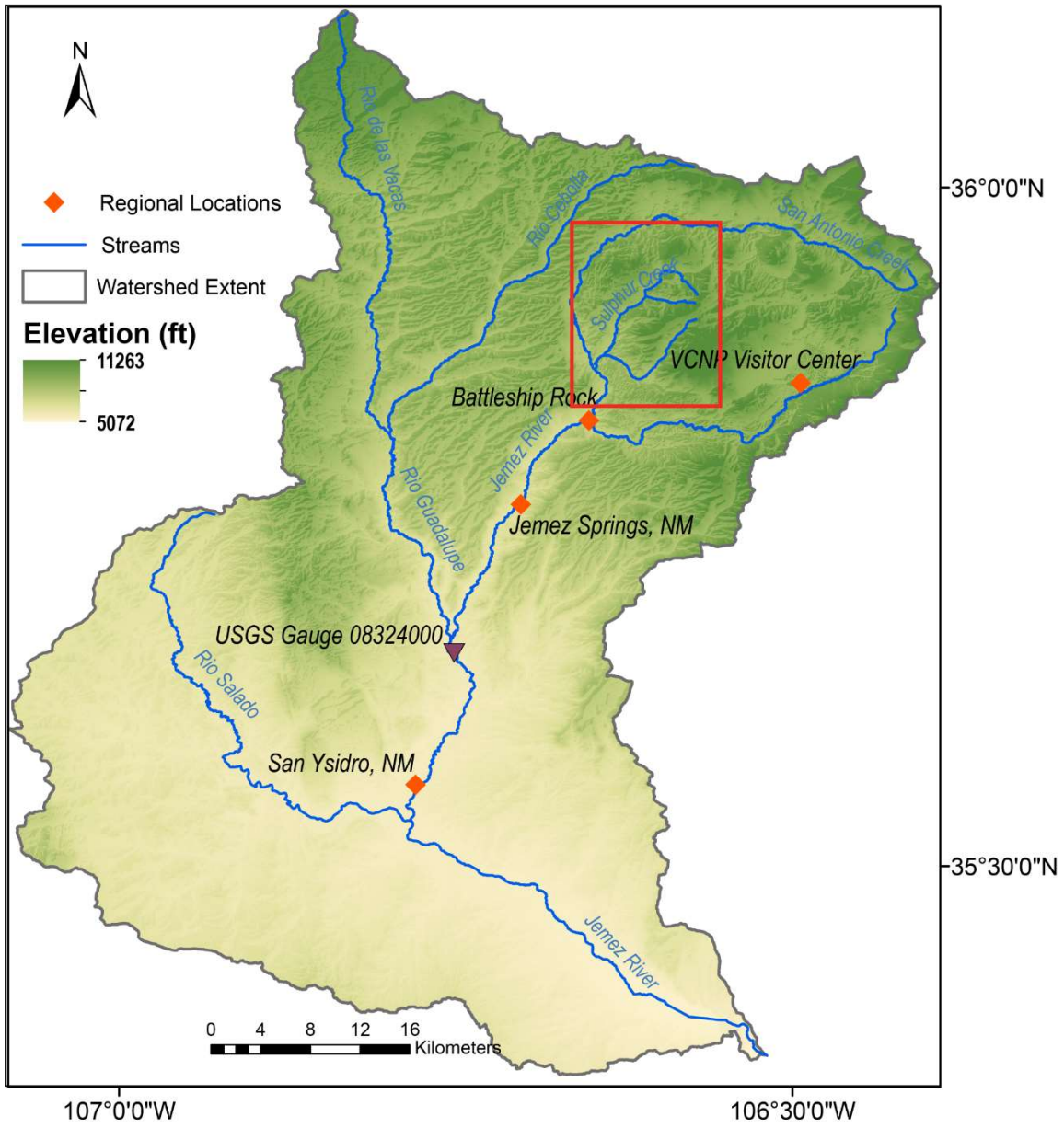

Figure 1. Digital Elevation Model and major surface streams of the Jemez River Watershed with regional locations displayed. Note the Sulphur Creek watershed on the flanks of the Valles Caldera resurgent dome. Rectangle identifies inset region displayed in Figure 6. Elevation data taken from USGS (2022) 3D Elevation Program 1/3 arc-second raster data. Hydrography data taken from USGS National Hydrography Dataset Best Resolution shapefile.

Figure 2

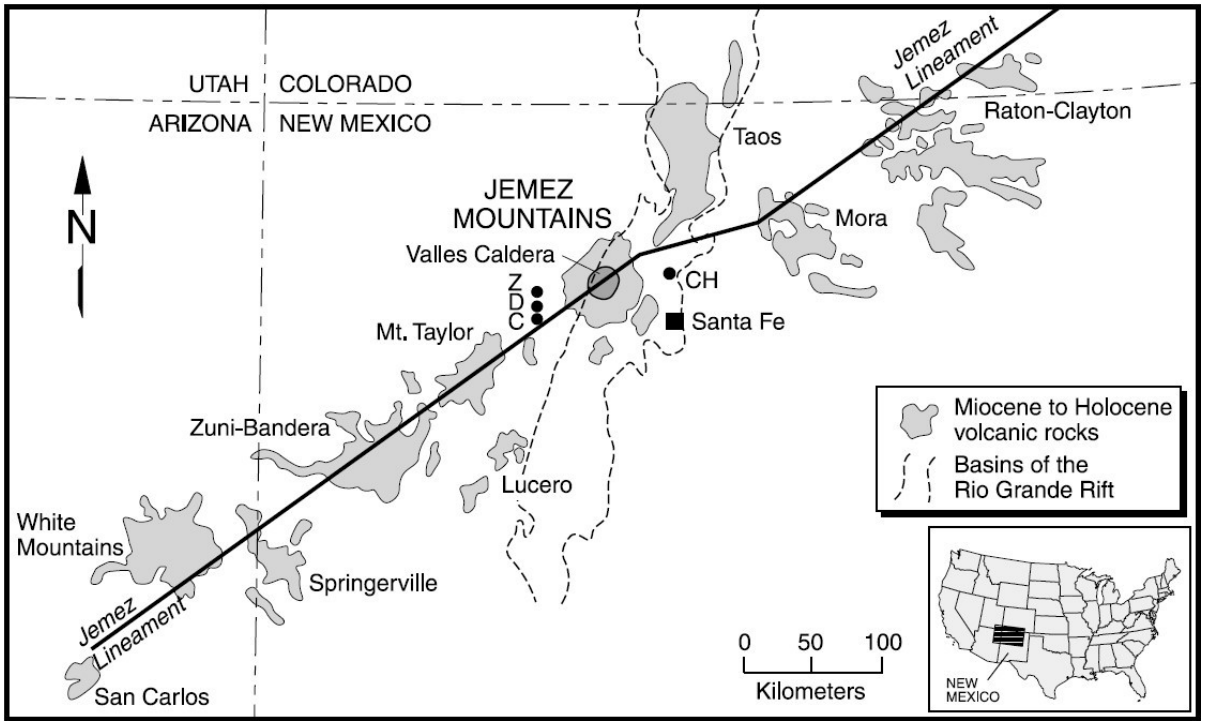

Figure 2. From Goff and Janik (2002) displaying the tectonic setting of the Valles Caldera at the intersection of the Jemez Lineament with the Rio Grande Rift.

Figure 3

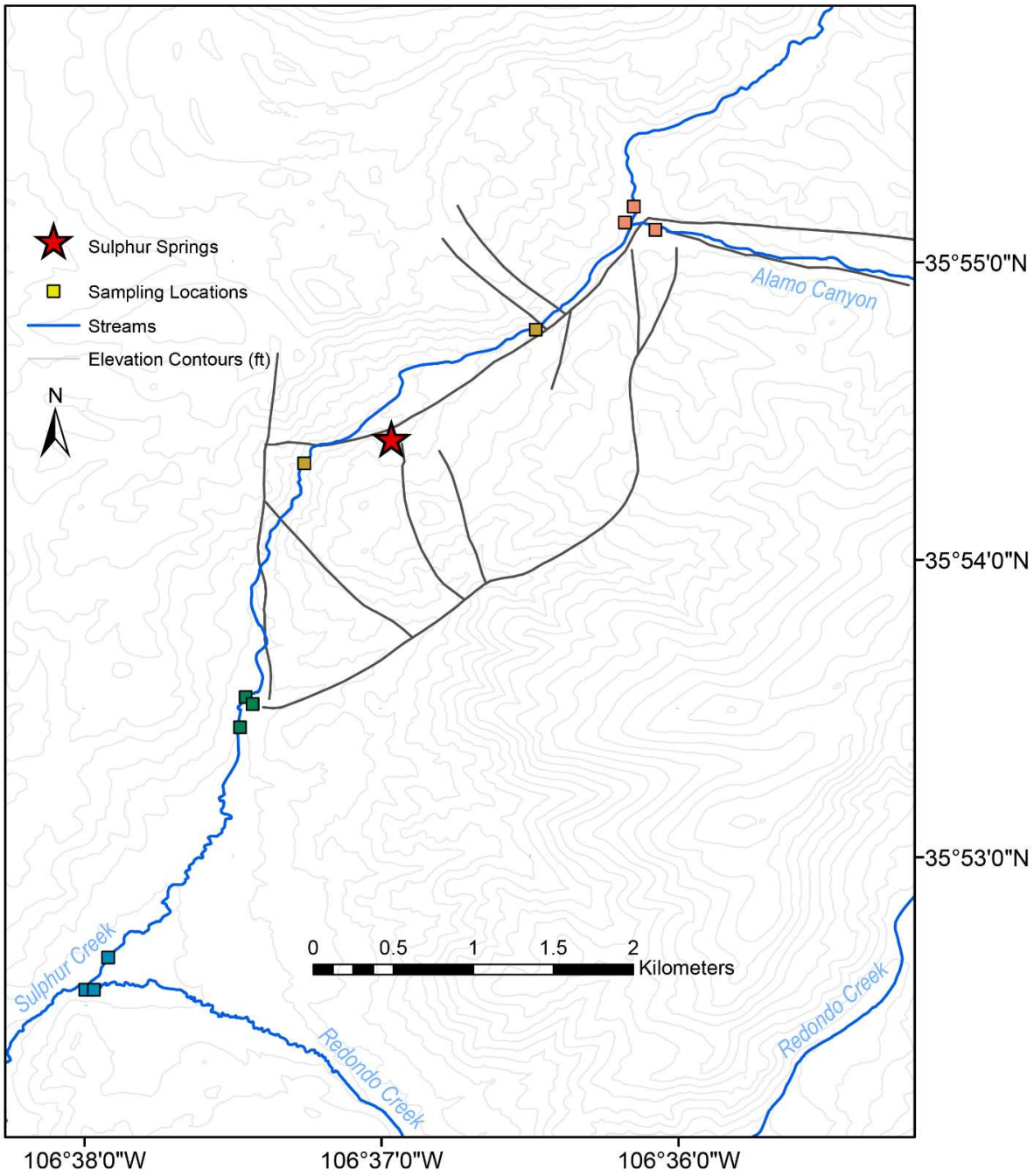

Figure 3. Structural map of selected faults in the Sulphur Springs area. Note the structural controls on the orientation of the canyons and location of geothermal features. Elevation data taken from USGS (2022) 3D Elevation Program 1/3 arc-second raster data. Hydrography data taken from USGS National Hydrography Dataset Best Resolution shapefile. Structural data taken from New Mexico Bureau of Geology and Mineral Resources OFGM 132 Valle San Antonio Geodatabase.

Figure 4

Figure 4. Note obvious leaching of surface gravels and general lack of vegetation near the geothermal features.

Figure 5

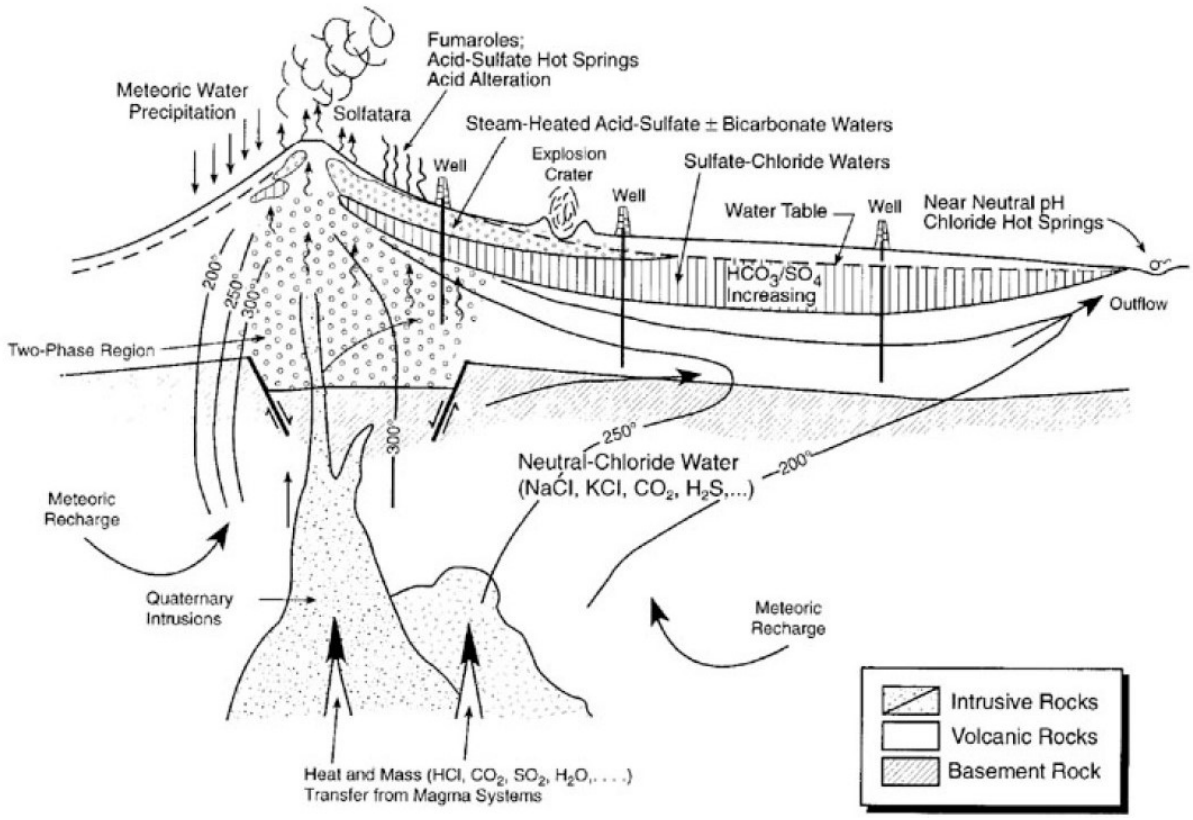

Figure 5. Young Igneous geothermal model as found in Goff and Janik (2000). Sulphur Springs is characteristic of the fumarolic and acid-sulfate environment denoted in the circle.

Figure 6

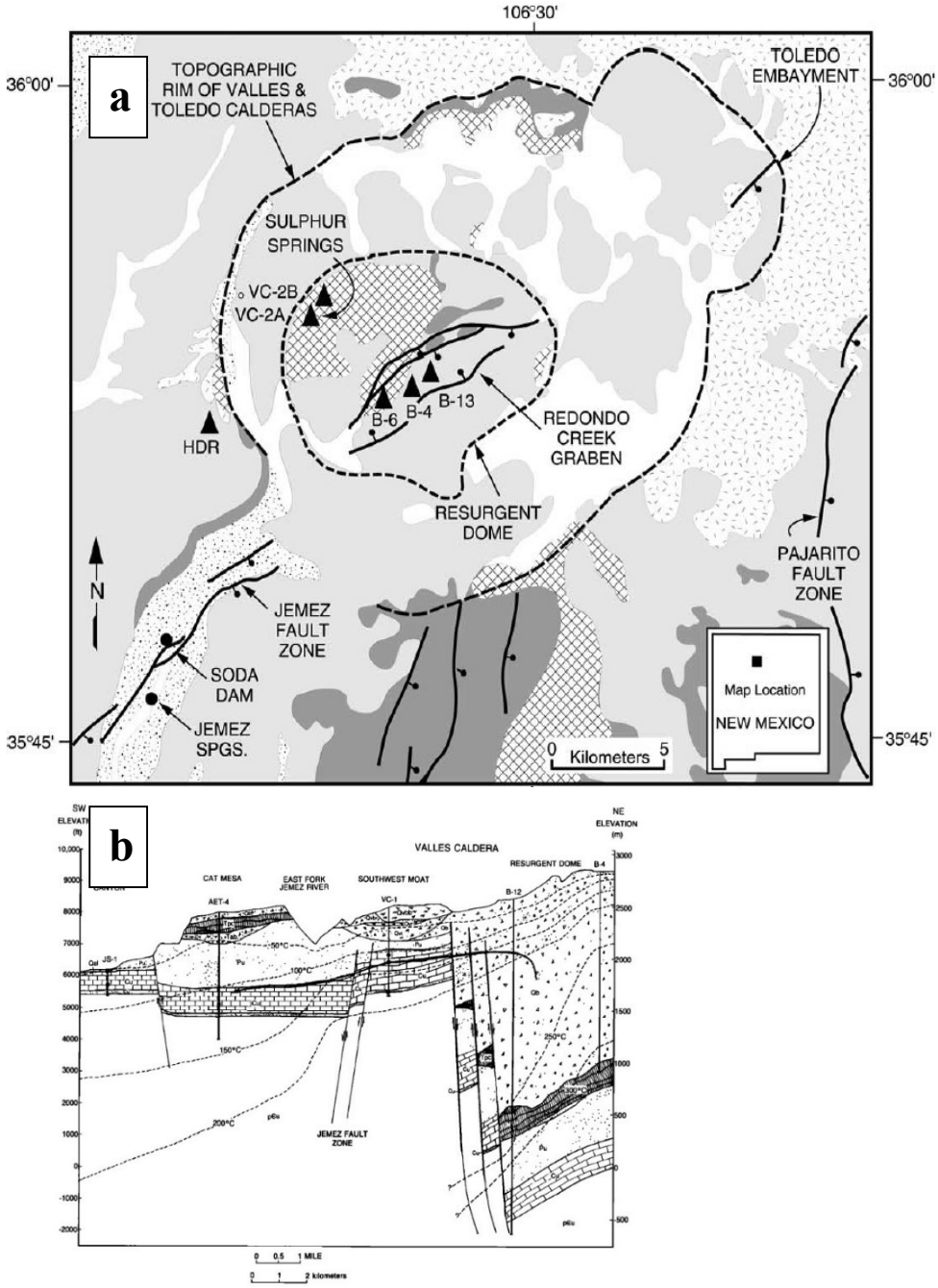

Figure 6 From Goff and Gardner (1994) and Goff and Janik (2002) showing a) the schematic Valles geology and b) cross-section beneath the Sulphur Springs area.

Figure 7

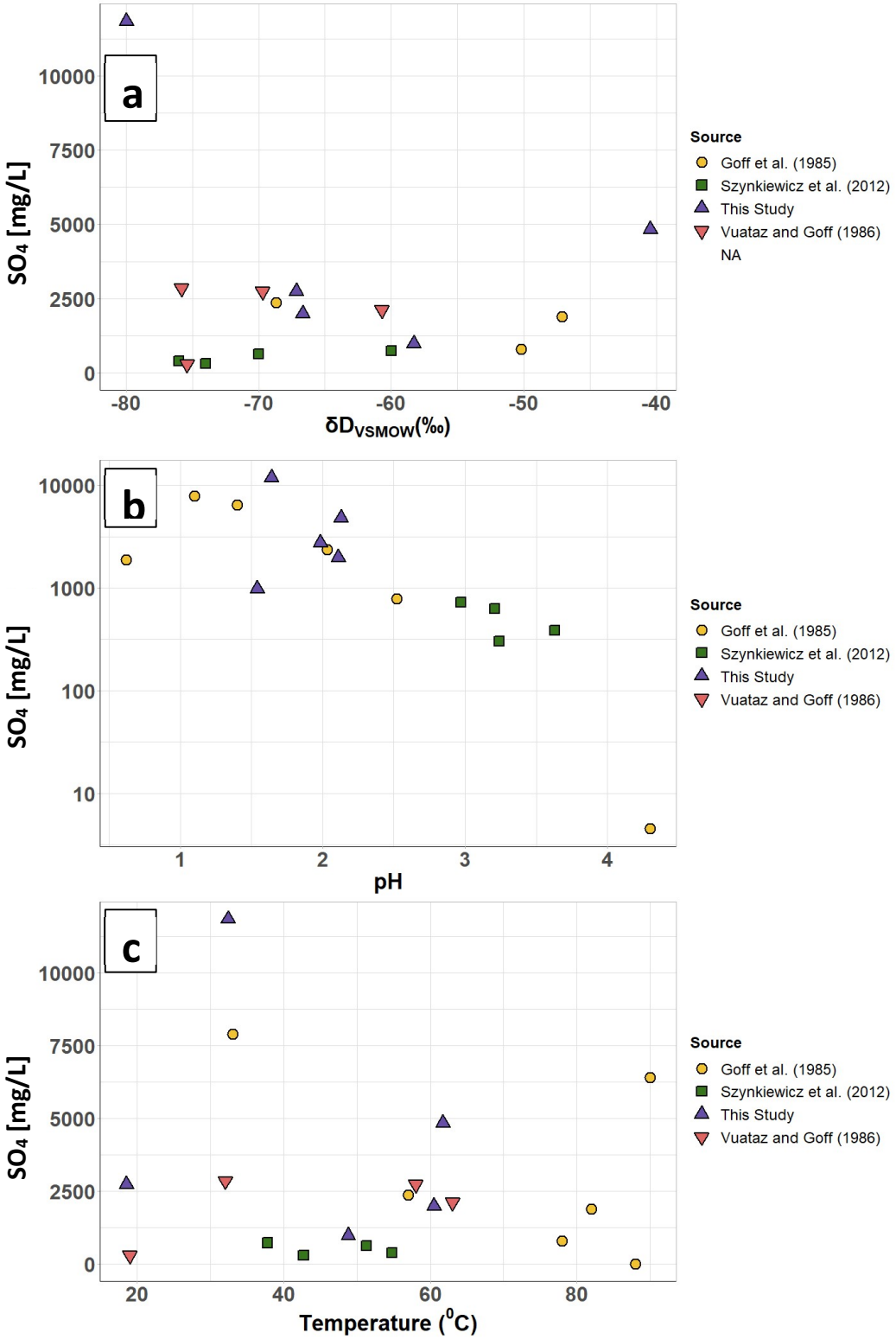

Figure 7 Summary of Sulphur Springs geochemistry through time and across three different studies in addition to this one (Goff et al. (1985); Vuataz and Goff (1986); Szynkiewicz et al. (2012).

Figure 8

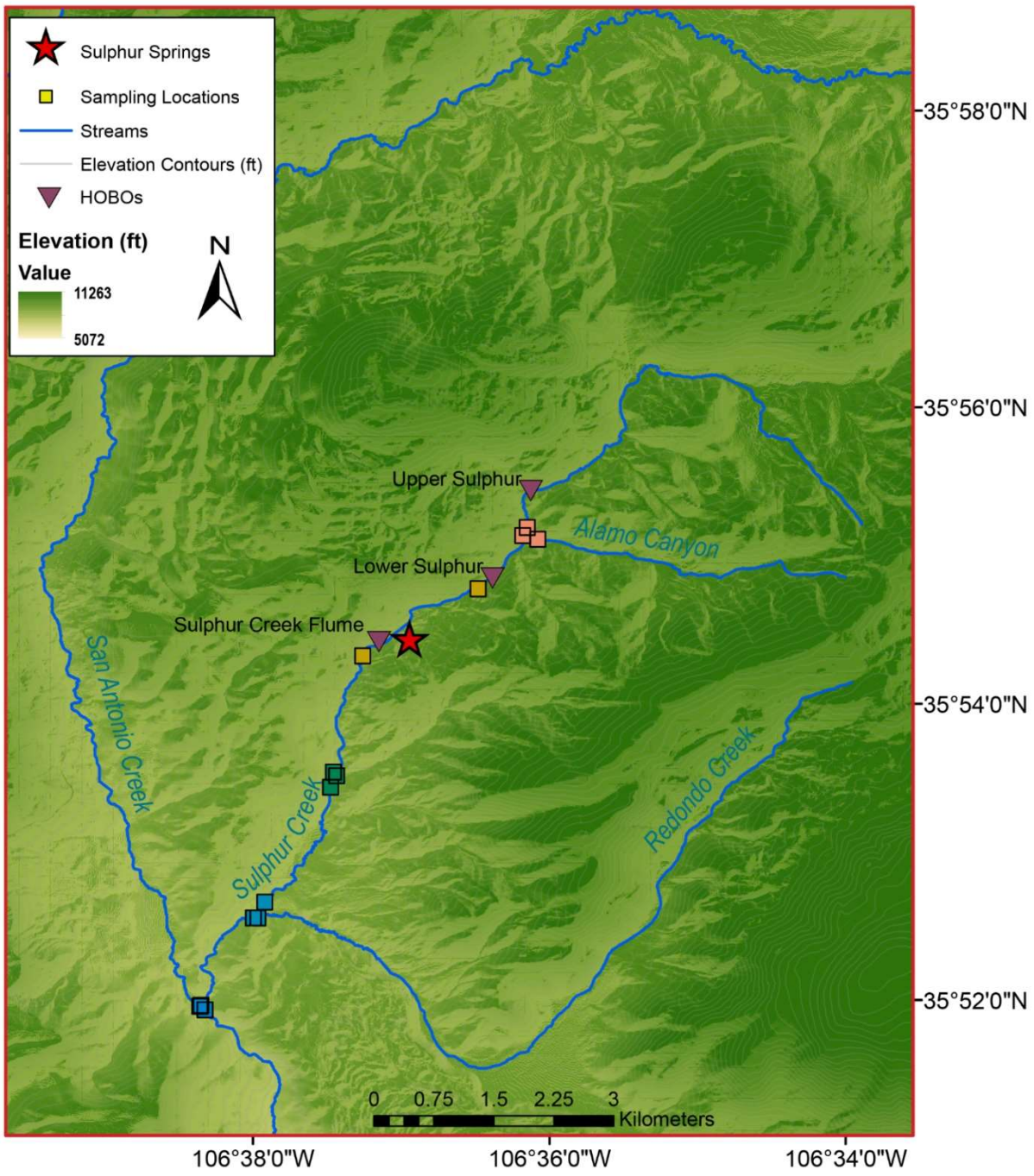

Figure 8. DEM of Sulphur Creek field area. Sampling locations are color coded based on their associated confluence. Red outline corresponds to inset marker in Figure 1. Elevation data taken from USGS (2022) 3D Elevation Program 1/3 arc-second raster data. Hydrography data taken from USGS National Hydrography Dataset Best Resolution shapefile.

Figure 9

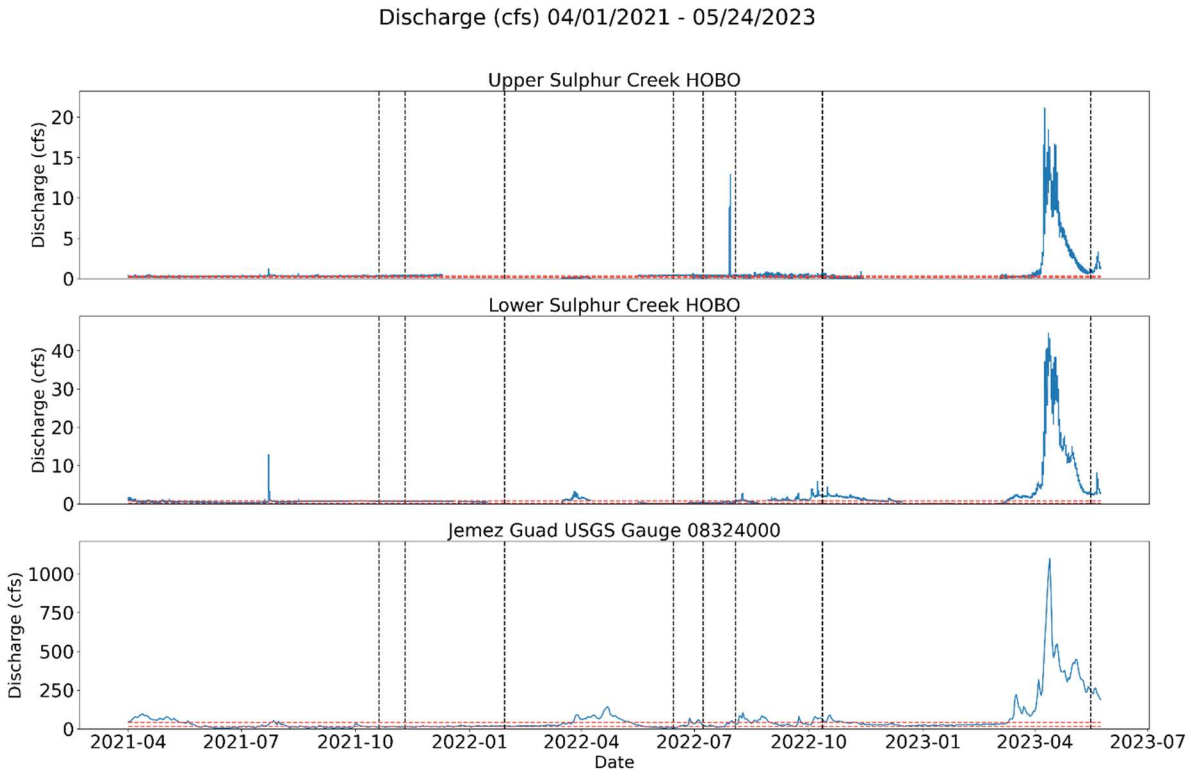

Figure 9. Hydrographs for gauging stations in Sulphur Creek and the Jemez River extending from April 1, 2021 to May 24, 2023. Horizontal red lines represent 25th and 75th percentile flows (calculated from previous 10 years of data).

Figure 10

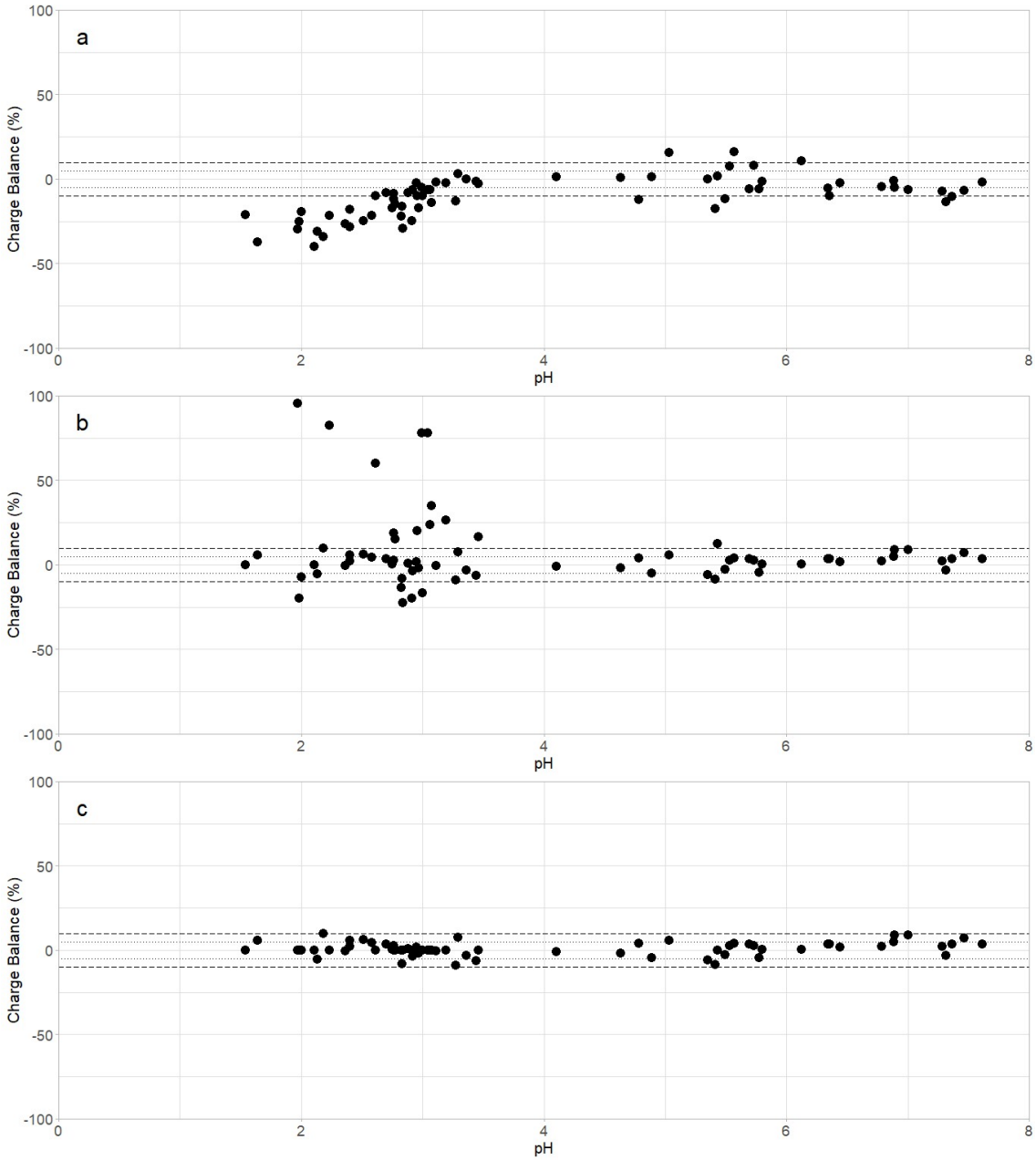

Figure 10. Charge balance error vs pH with: a) unaltered major ion concentrations, b) major ion concentrations with SO_4^{2-} /HSO_4^- partitioning, and c) geochemical modelling to handle outstanding unbalanced samples

Figure 11

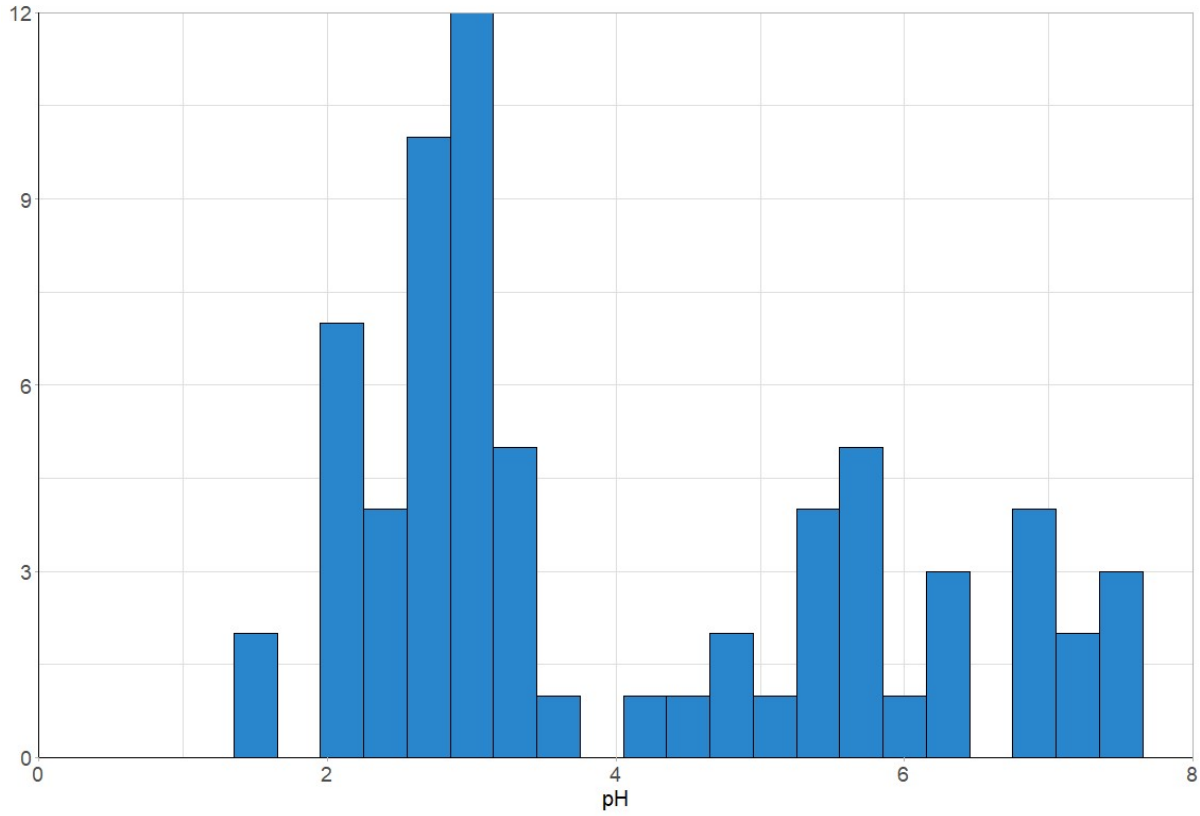

Figure 11. Histogram of pH values collected in this study. Note the concentration of samples falling between pH 2 and 3.5 and the secondary peak of samples falling between pH 5 and 7

Figure 12

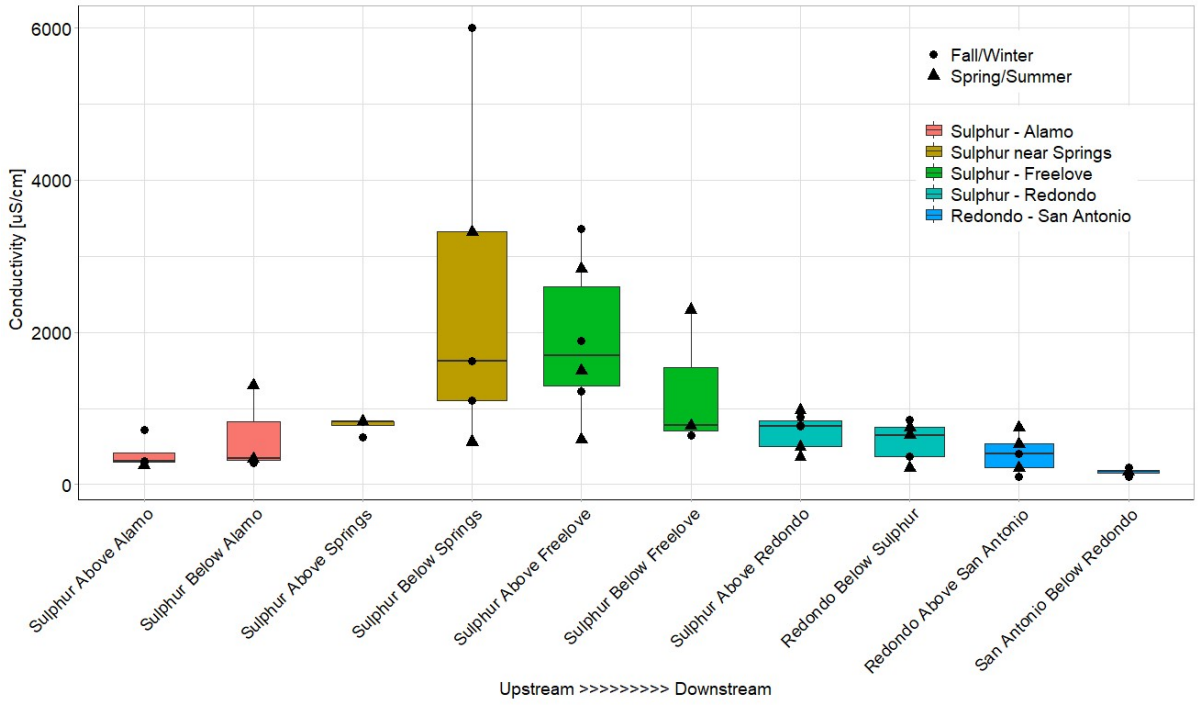

Figure 12 Box plot displaying conductivity at all sample sites in the main stem. Sample sites are arranged such that upstream to downstream samples sites appear from left to right. Note the peak in-stream conductivity occurs at/immediately below Sulphur Springs.

Figure 13

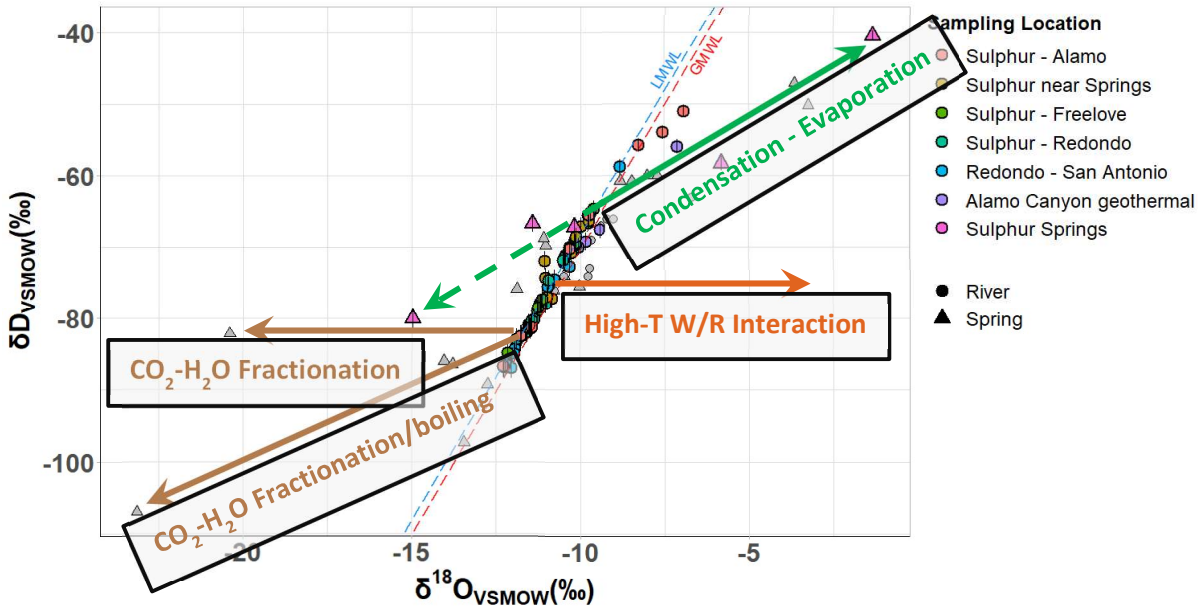

Figure 13. Stable Isotope Plot for samples collected for this and previous studies. Samples collected in this study are shown by the colored points, while previous data are displayed with the grey fill. Note the divergence of several Sulphur Springs samples from the Meteoric Water Line. δD analytical errors are displayed on each point, while $\delta^{18}O$ analytical error is within the area of the data points. Previous data are taken from Vuataz and Goff (1986) and Szynkiewicz et al. (2012).

Figure 14

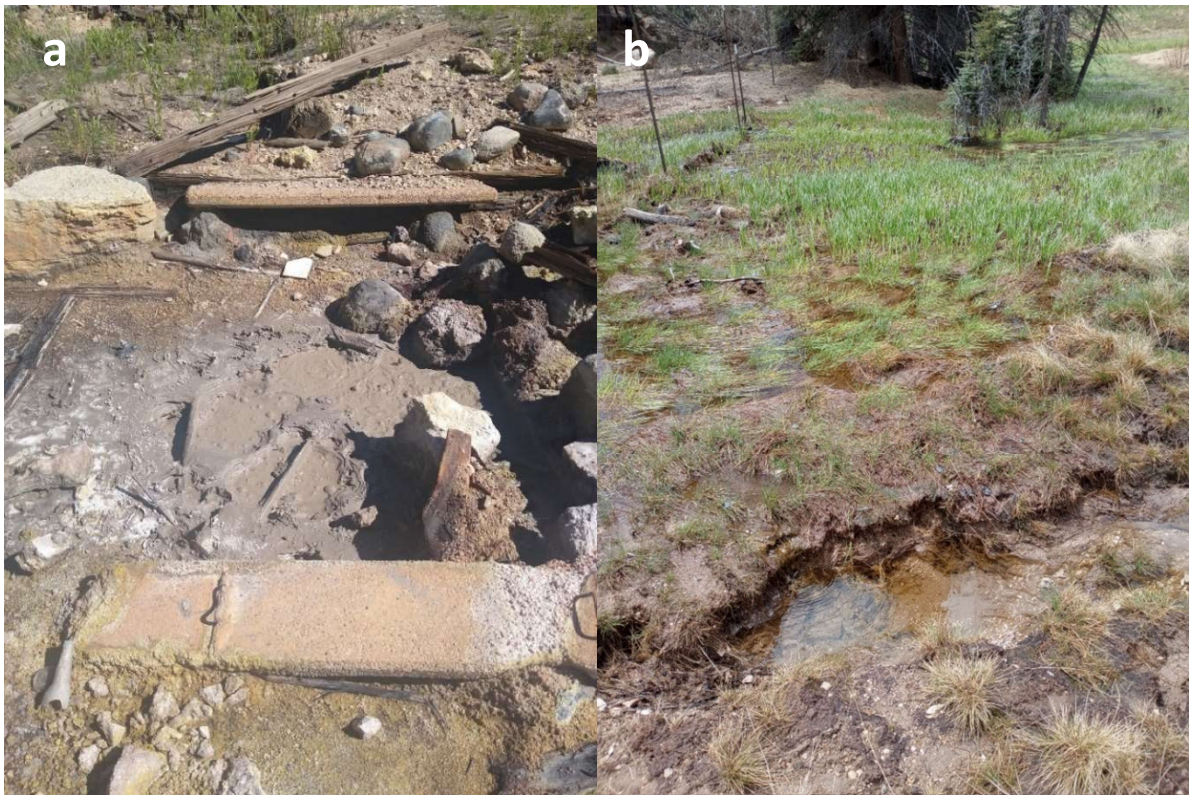

Figure 14. Site photos from A) Men's Bathhouse Mudpot in the Sulphur Springs area and B) The Alamo Canyon – Sulphur Creek confluence. Note the evident bubbling in the mudpot and the boggy conditions at the Alamo Canyon confluence. Both of these samples show evaporation trends in the stable isotope plot.

Figure 15

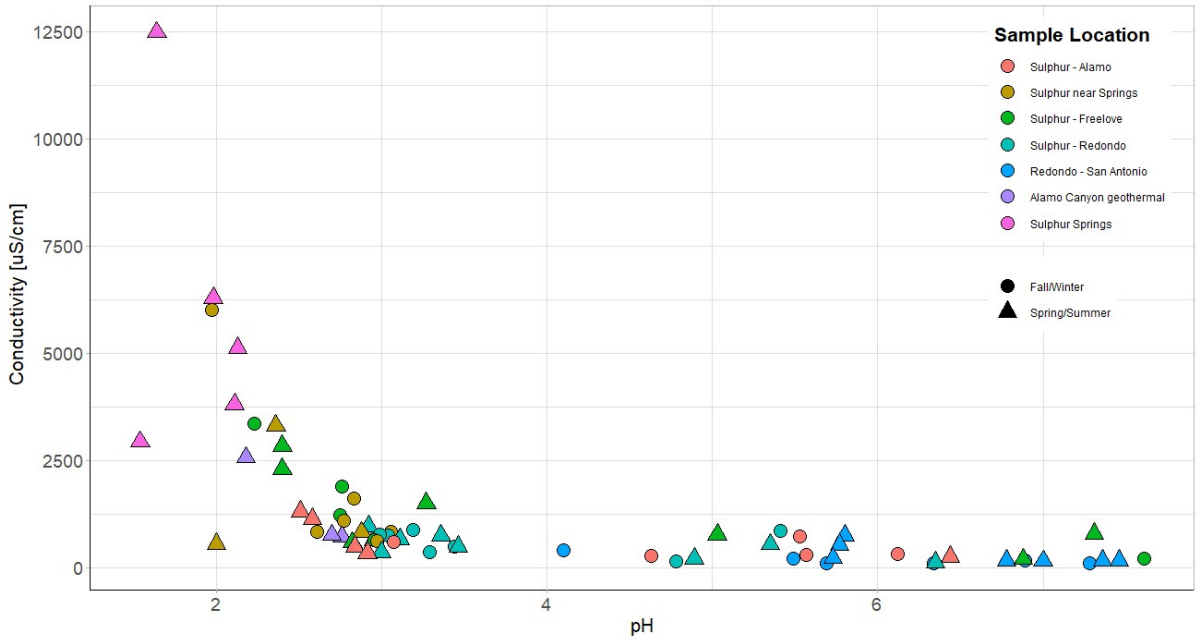

Figure 15. Electrical conductivity and pH display a negative relationship. Highly-conductive waters are found at the lowest pH values in the field area. High-pH waters have the lowest conductivities in the field area.

Figure 16

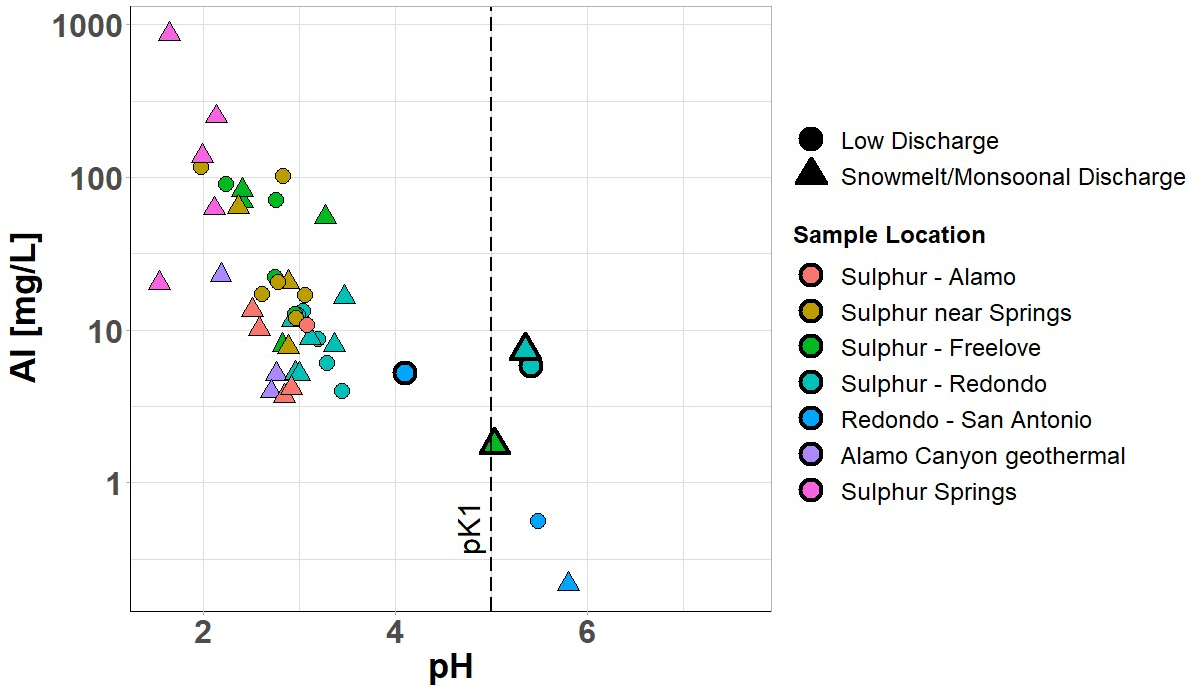

Figure 16. Relationship of in-stream Al concentrations to sample pH. Note the change in behavior on either side of pH 5 (corresponding to pK_1 for hydrolysis of Al). Boldly-outlined data points represent samples supersaturated with respect to alunite ($KAl_3(SO_4)_2(OH)_6$).

Figure 17

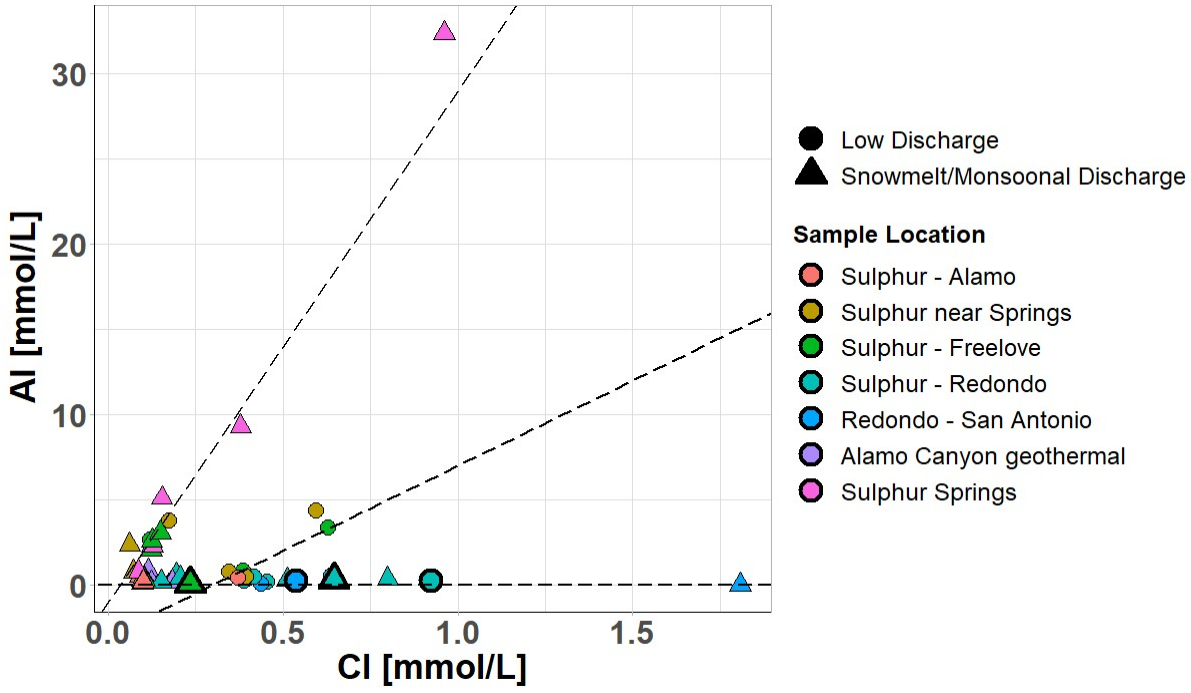

Figure 17. Relationship of Al to Cl in the field area. Note the origin of waters downstream of Sulphur Springs as due to mixing between relatively fresh Alamo Canyon waters and Sulphur Springs waters. Low-Al, high-Cl samples were collected at fresh tributaries in the field area. Alunite supersaturation is expressed with the bold outline.

Figure 18

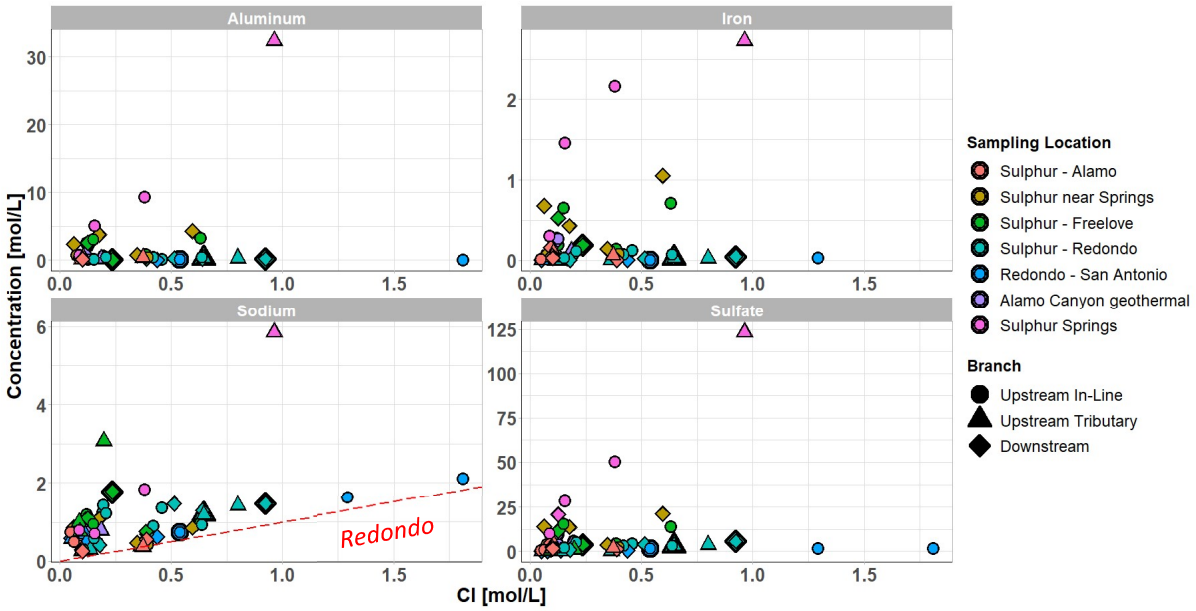

Figure 18 Displaying Solute-chloride relationships for aluminum, iron, sodium, and sulfate. Note that a suite of samples in Na-Cl space follows the 1:1 line (red), suggesting halite controls the Na:Cl in this subset of data (see discussion in text). These plots utilize all samples collected in the study and are not separated by date. All samples categorized under Sulphur Springs are taken from acid-sulfate vents, not streams.

Figure 19

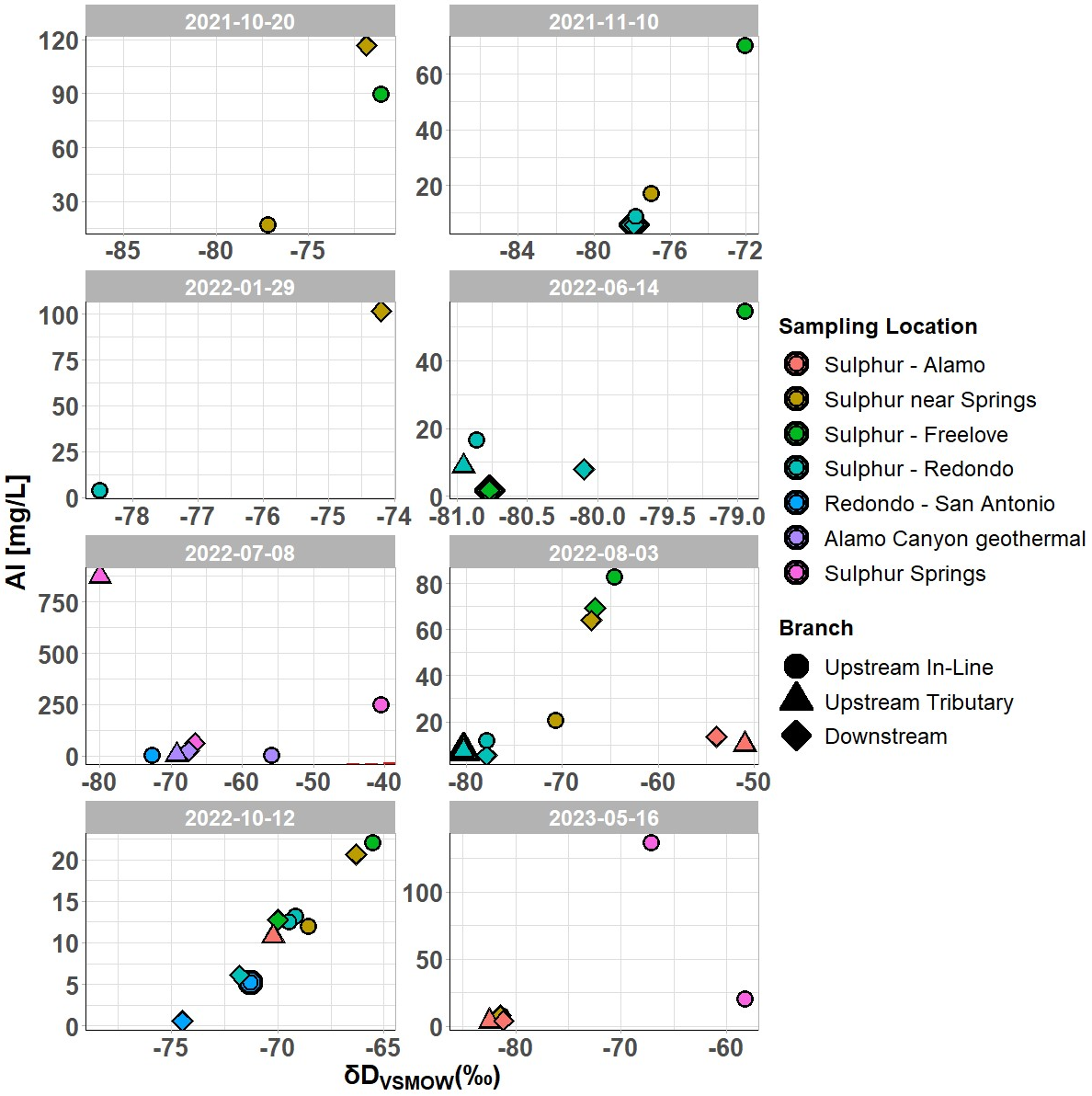

Figure 19 Al-δD compositions for dates with full suite of data available. Note that most downstream samples (diamonds) fall along conservative mixing lines between the upstream tributary samples. On 8/3/2022, the Sulphur – Redondo cluster shows an upstream sample that is supersaturated with respect to alunite and the downstream sample does not fall along a conservative mixing line between the tributaries. This possibly indicates an observable non-conservative process like mineral precipitation.

Figure 20

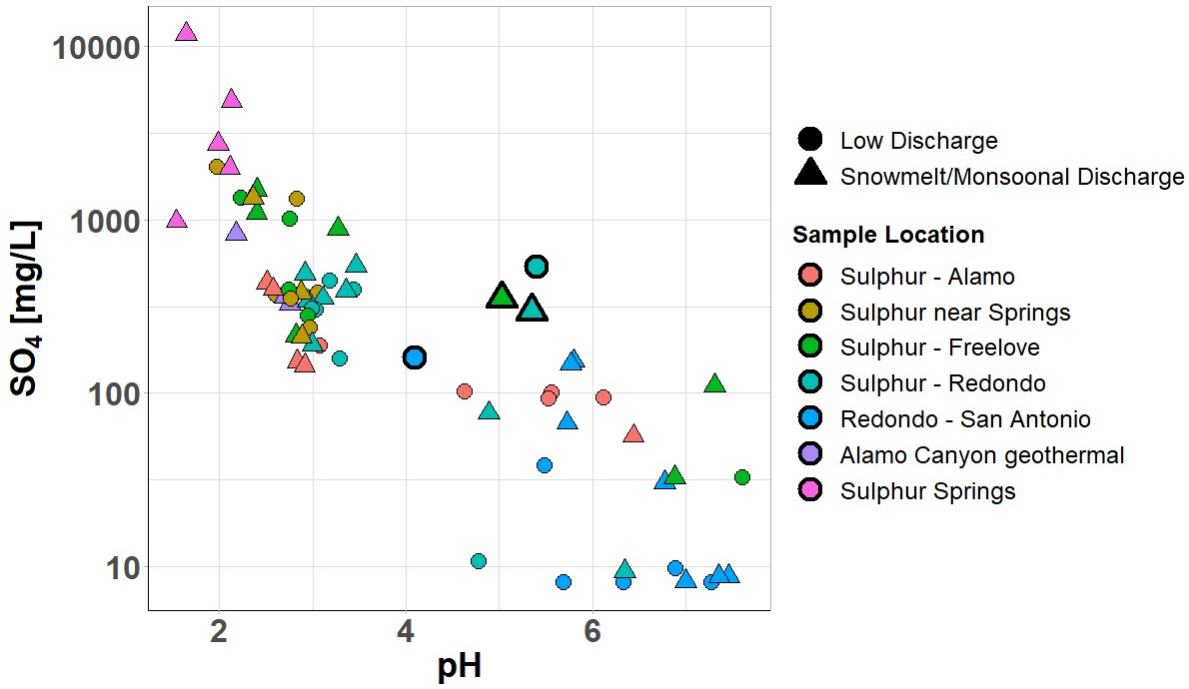

Figure 20 Relationship of log SO_4 concentration to pH. The highest SO_4 concentrations are found at low pH, which follows from the fact that SO_4 is the primary aqueous ion in Sulphur Springs fluids and is the primary source of acidity in the acid-sulfate geothermal system.

Figure 21

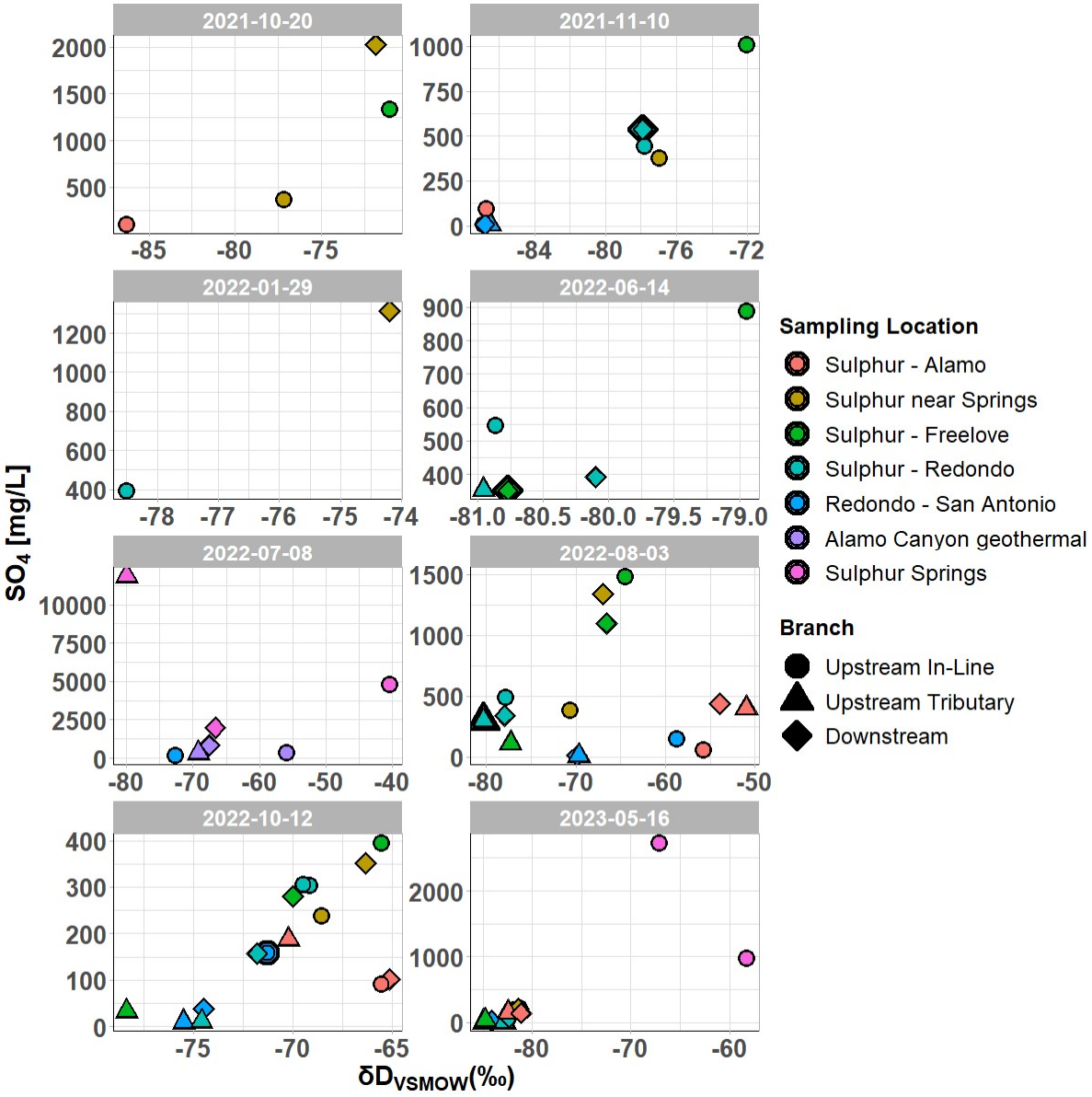

Figure 21. SO_4-δD compositions for all samples. Similar relationships to Al. Downstream samples tend to lie along conservative mixing lines between the two upstream tributary samples. Note that Alamo Canyon waters generally fall to the low-SO_4, high-δD quadrant of the graph. The high-δD in these samples is due to surface evaporation of waters at this site.

Figure 22

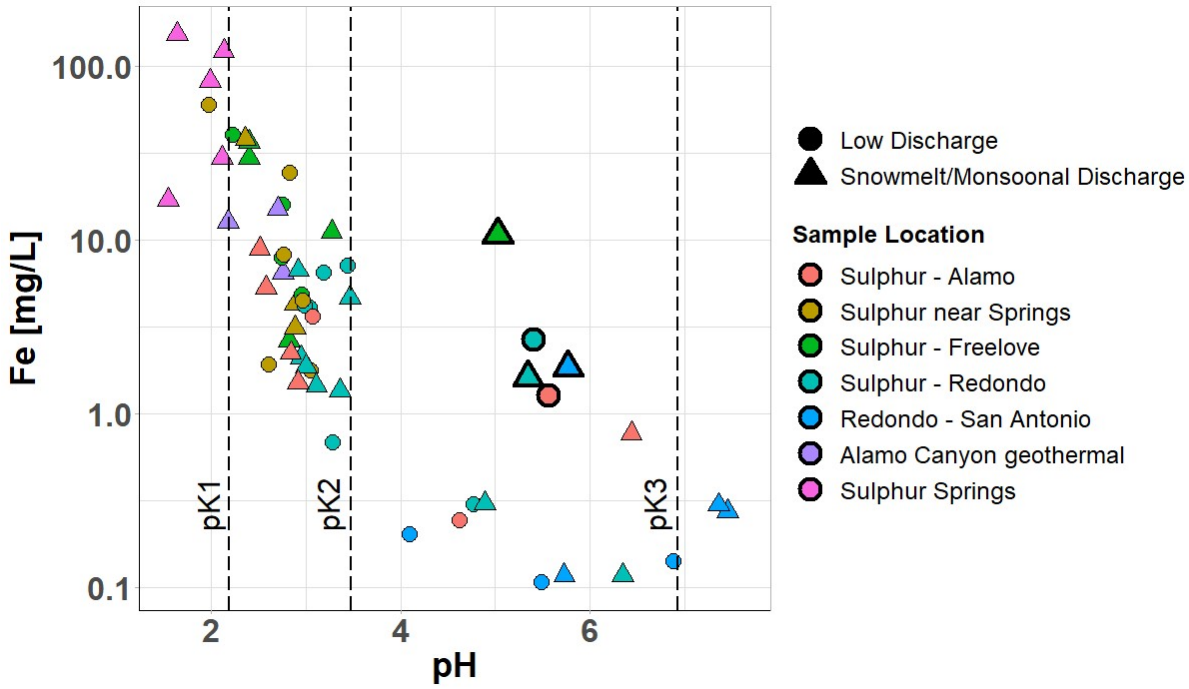

Figure 22 Relationship between Fe and pH. Hydrolysis constants are overlain on the data points. Most measurable Fe concentrations are found at pH < pK2, however the only samples modelled to be supersaturated with respect to goethite (FeOOH) are at pK2 < pH < pK3.

Figure 23

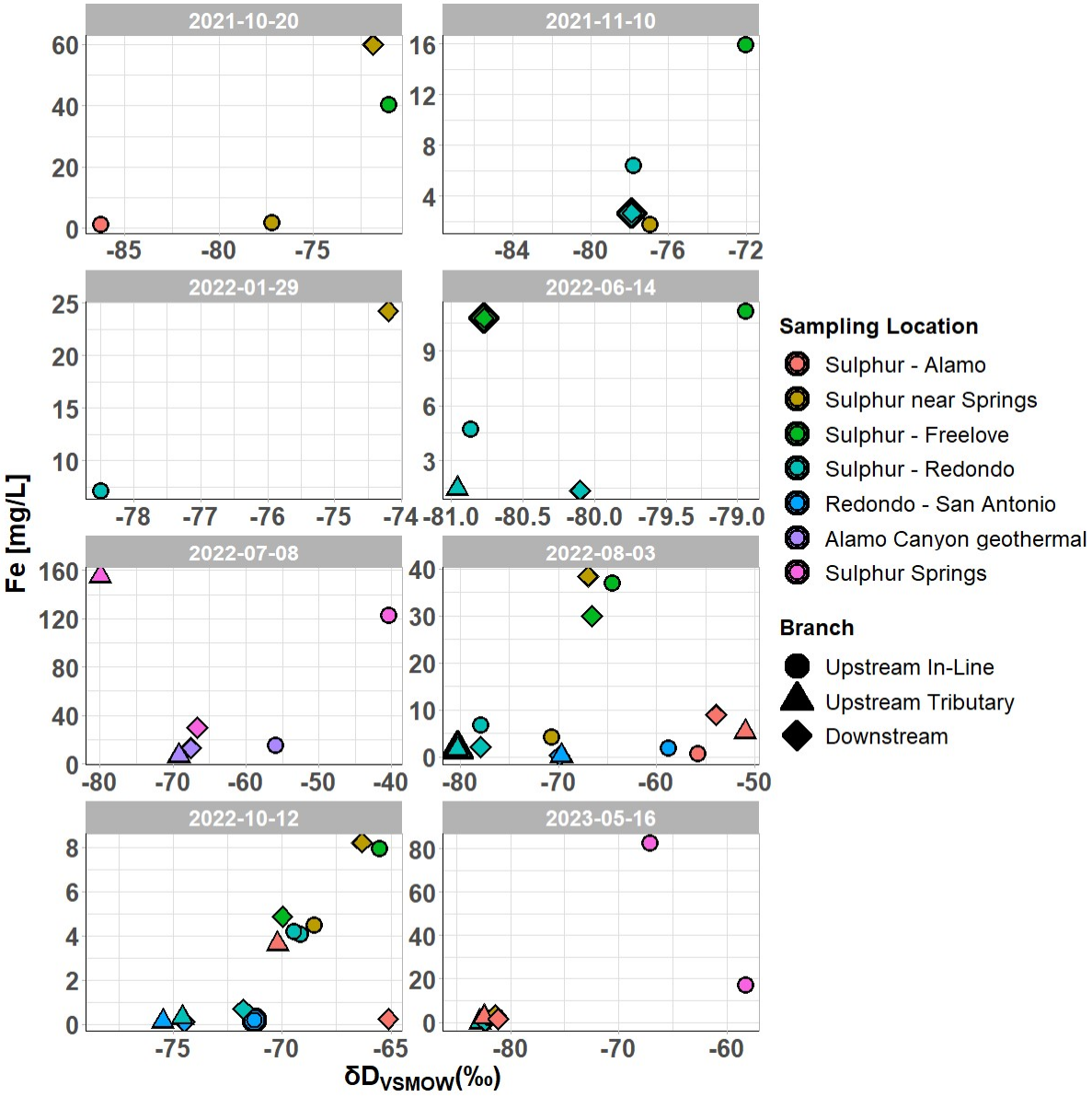

Figure 23 Fe-δD compositions divided by collection dates. Limited to dates with a full suite of samples collected. Similar relationships to Al and SO_4 identified. Supersaturation mineral assessed in this plot is goethite (FeO(OH)). The 8/3/2022 Sulphur – Redondo cluster shows similar relationships to Al and SO_4 with alunite, suggesting that non-conservative processes are occurred at this sample site on that date.

Figure 24

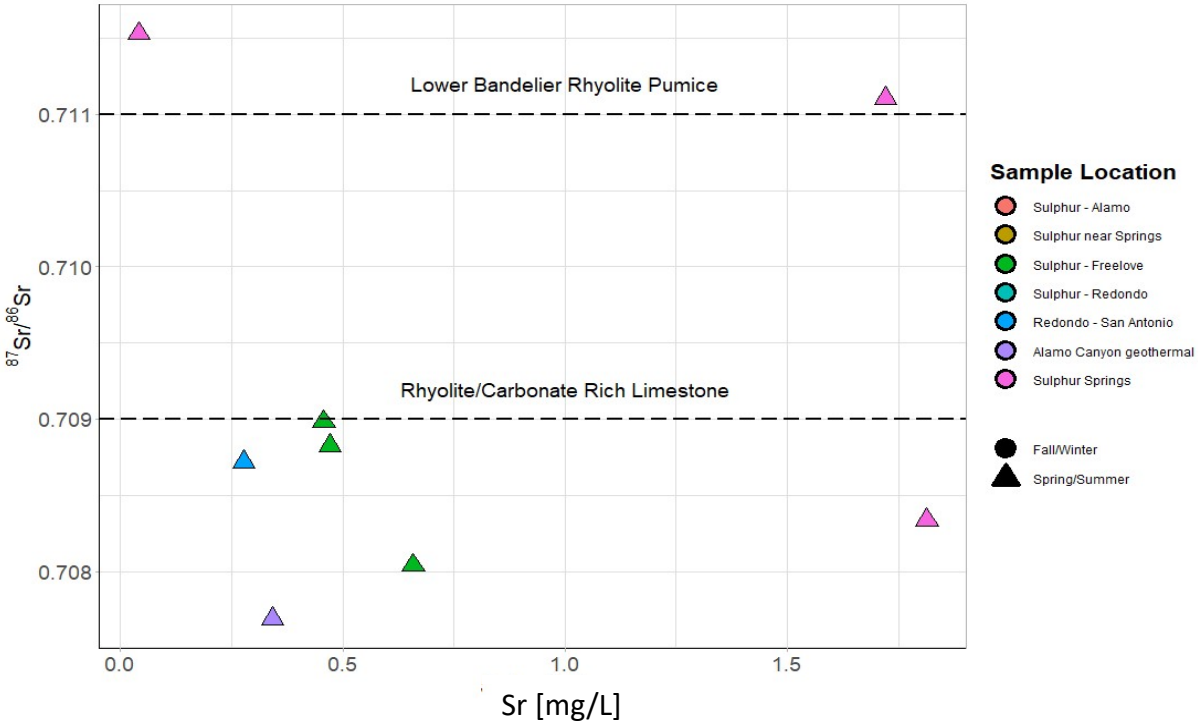

Figure 24. Sr composition of selected waters. $^{87}Sr/^{86}Sr$ for significant Valles lithological units are taken from Vuataz et al. (1988).

Figure 25

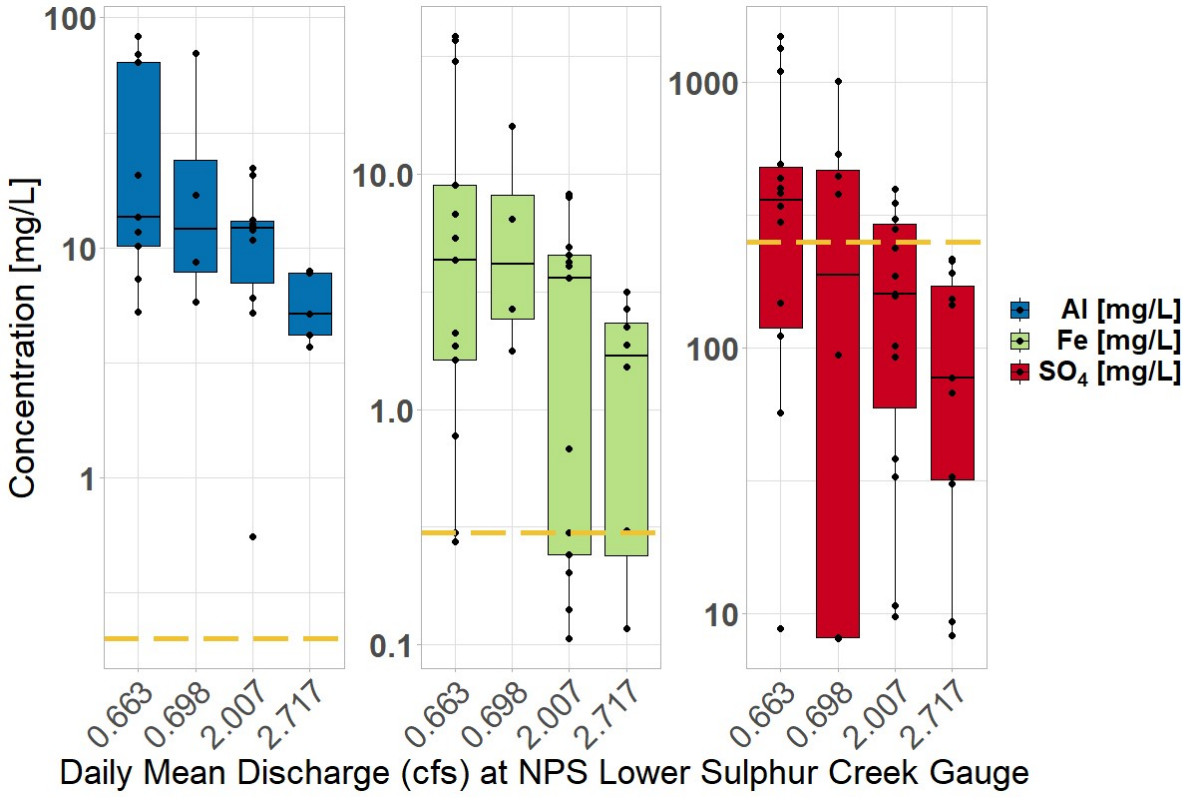

Figure 25. Relationship between discharge at Lower Sulphur gauge and stream composition throughout the field area. EPA Secondary Drinking Water regulations for each solute displayed as dashed yellow line (EPA, 2023). Springs samples not considered as they are less impacted by discharge conditions.

Appendix 1

Color-scaled maps detailing changes in geochemical parameters across the field site on various dates.

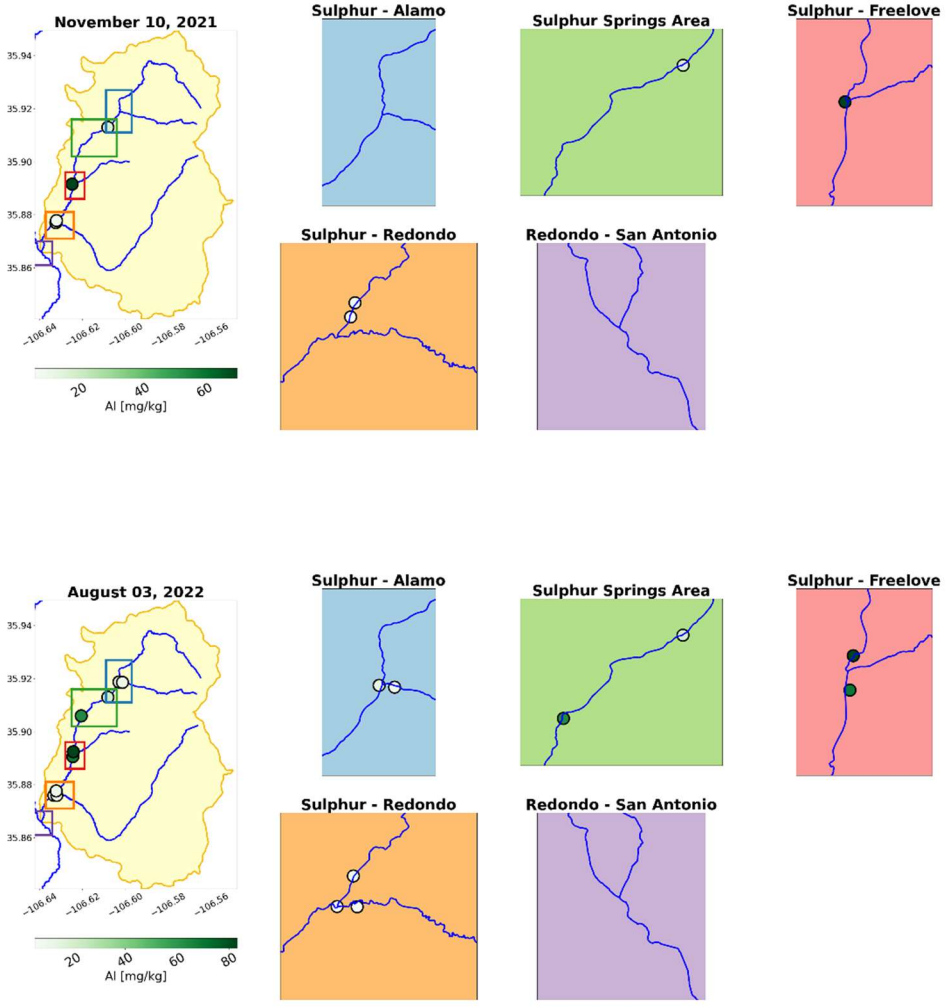

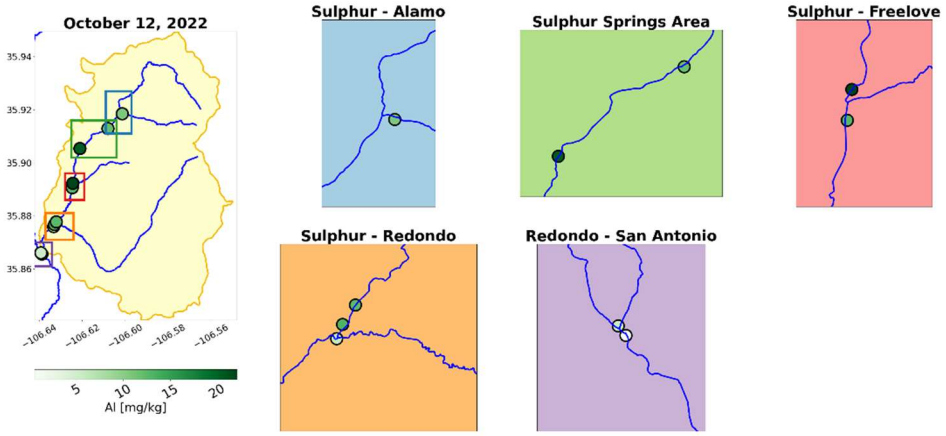
October 12, 2022
35.94
35.92
35.90
35.88
35.86
−106.64
−106.62
−106.60
−106.58
−106.56
5
10
15
20
Al [mg/kg]
Sulphur - Alamo
Sulphur Springs Area
Sulphur - Freelove
Sulphur - Redondo
Redondo - San Antonio

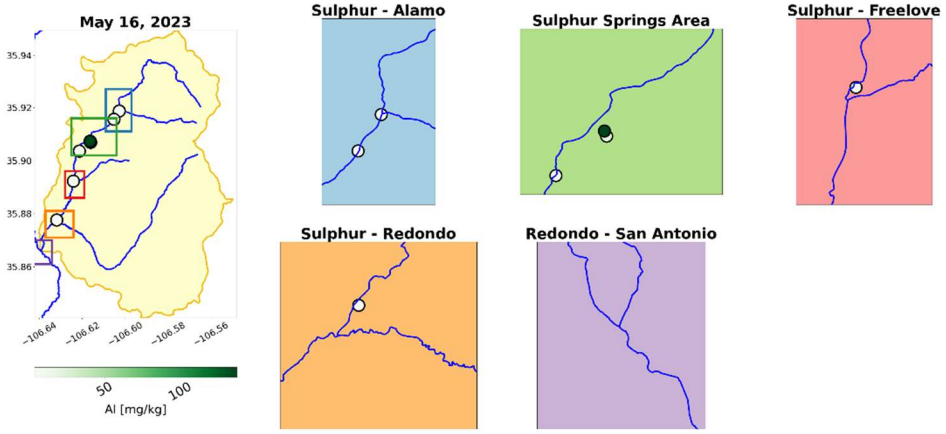
May 16, 2023
35.94
35.92
35.90
35.88
35.86
−106.64
−106.62
−106.60
−106.58
−106.56
50
100
Al [mg/kg]
Sulphur - Alamo
Sulphur Springs Area
Sulphur - Freelove
Sulphur - Redondo
Redondo - San Antonio

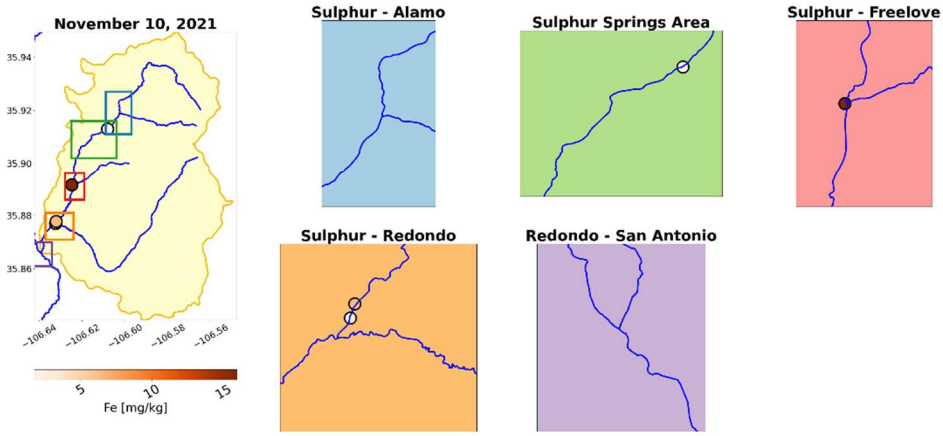
November 10, 2021
35.94
35.92
35.90
35.88
35.86
−106.64
−106.62
−106.60
−106.58
−106.56
5
10
15
Fe [mg/kg]
Sulphur - Alamo
Sulphur Springs Area
Sulphur - Freelove
Sulphur - Redondo
Redondo - San Antonio

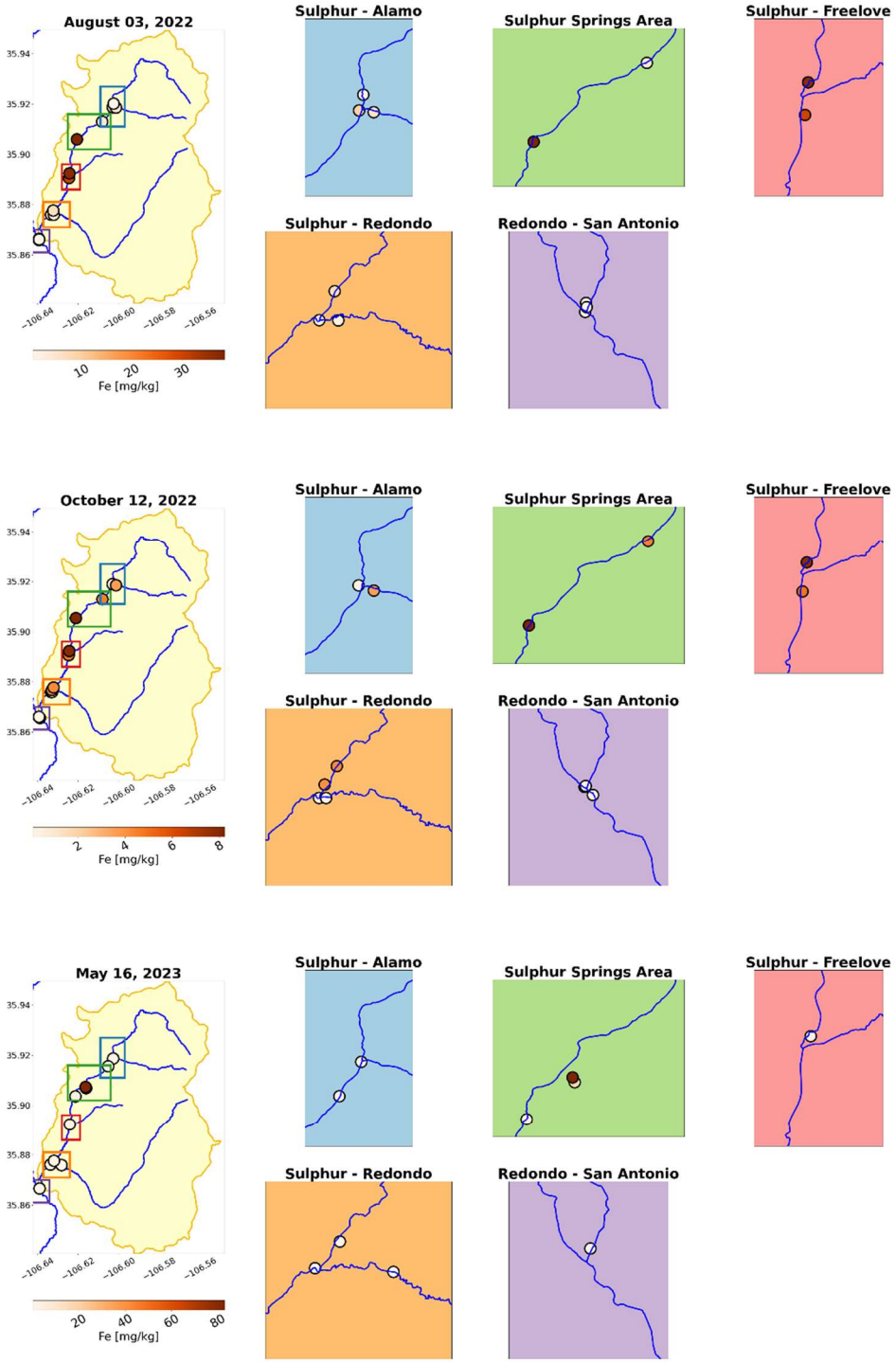
August 03, 2022
35.94
35.92
35.90
35.88
35.86
−106.64
−106.62
−106.60
−106.58
−106.56
10
20
30
Fe [mg/kg]
Sulphur - Alamo
Sulphur Springs Area
Sulphur - Freelove
Sulphur - Redondo
Redondo - San Antonio
October 12, 2022
35.94
35.92
35.90
35.88
35.86
−106.64
−106.62
−106.60
−106.58
−106.56
2
4
6
8
Fe [mg/kg]
Sulphur - Alamo
Sulphur Springs Area
Sulphur - Freelove
Sulphur - Redondo
Redondo - San Antonio
May 16, 2023
35.94
35.92
35.90
35.88
35.86
−106.64
−106.62
−106.60
−106.58
−106.56
20
40
60
80
Fe [mg/kg]
Sulphur - Alamo
Sulphur Springs Area
Sulphur - Freelove
Sulphur - Redondo
Redondo - San Antonio

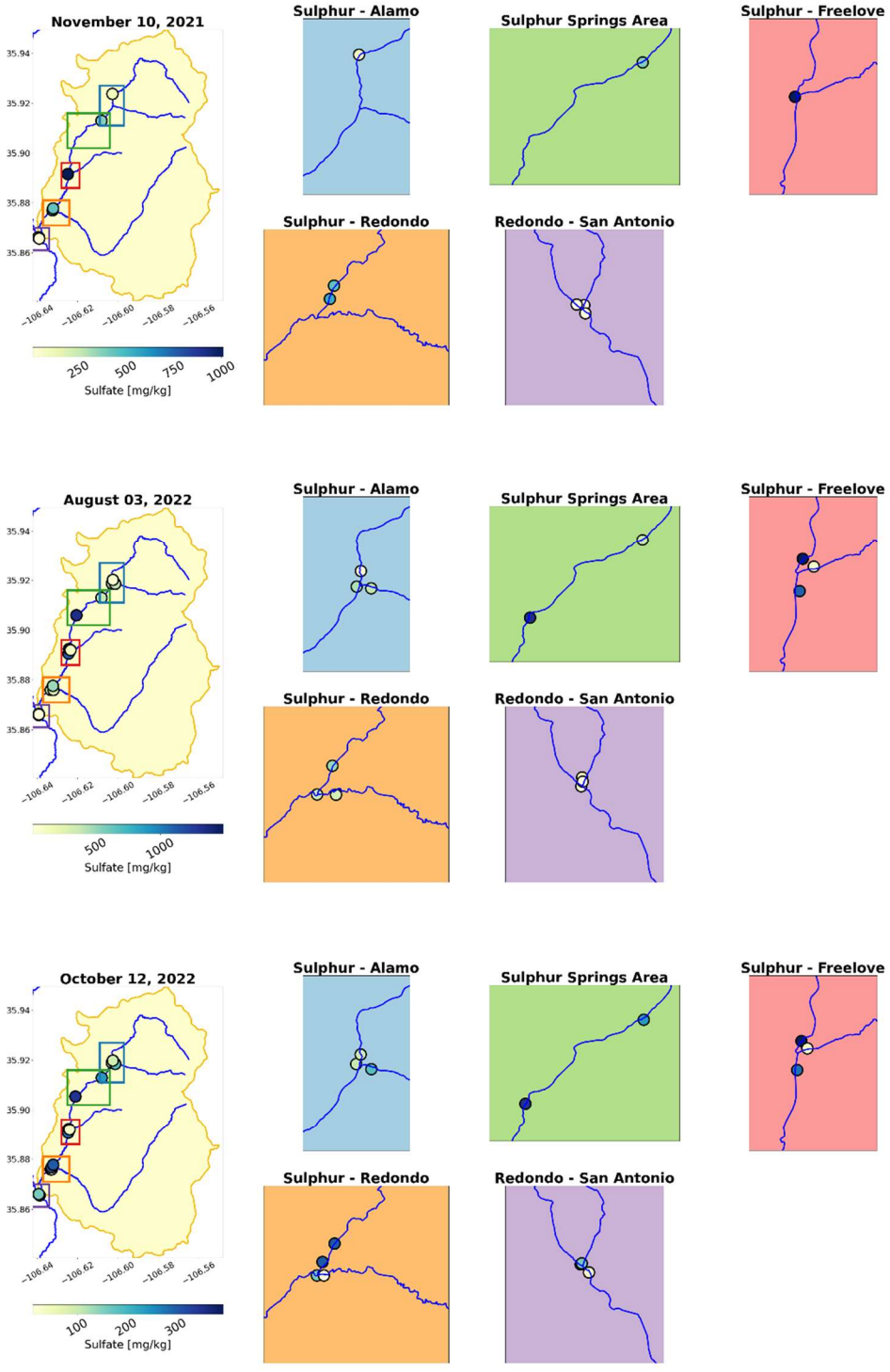
November 10, 2021
35.94
35.92
35.90
35.88
35.86
−106.64
−106.62
−106.60
−106.58
−106.56
250
500
750
1000
Sulfate [mg/kg]
Sulphur - Alamo
Sulphur Springs Area
Sulphur - Freelove
Sulphur - Redondo
Redondo - San Antonio
August 03, 2022
35.94
35.92
35.90
35.88
35.86
−106.64
−106.62
−106.60
−106.58
−106.56
500
1000
Sulfate [mg/kg]
Sulphur - Alamo
Sulphur Springs Area
Sulphur - Freelove
Sulphur - Redondo
Redondo - San Antonio
October 12, 2022
35.94
35.92
35.90
35.88
35.86
−106.64
−106.62
−106.60
−106.58
−106.56
100
200
300
Sulfate [mg/kg]
Sulphur - Alamo
Sulphur Springs Area
Sulphur - Freelove
Sulphur - Redondo
Redondo - San Antonio

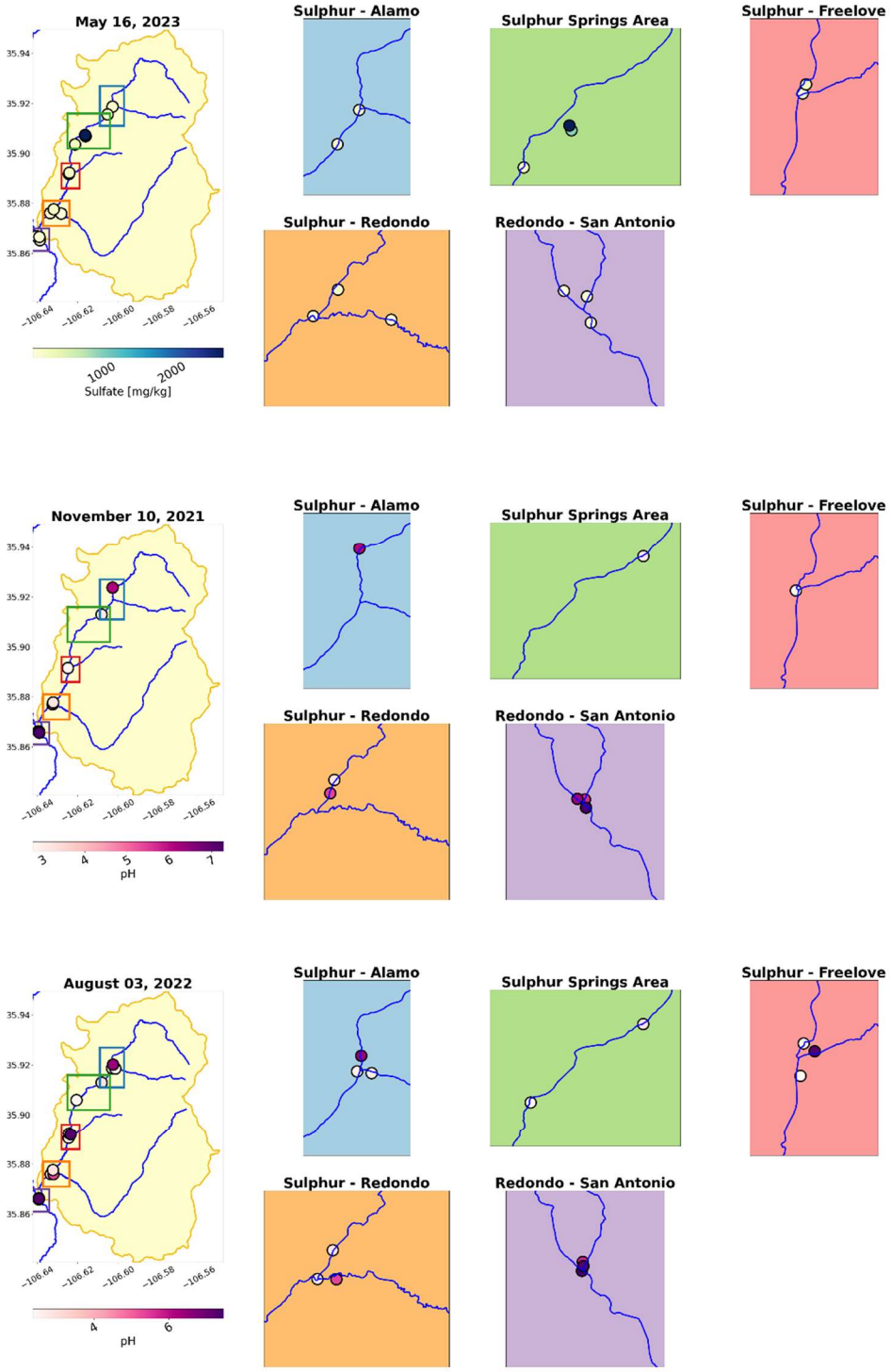
May 16, 2023
35.94
35.92
35.90
35.88
35.86
−106.64
−106.62
−106.60
−106.58
−106.56
1000
2000
Sulfate [mg/kg]
Sulphur - Alamo
Sulphur Springs Area
Sulphur - Freelove
Sulphur - Redondo
Redondo - San Antonio
November 10, 2021
3
4
5
6
7
pH
August 03, 2022
4
6
pH

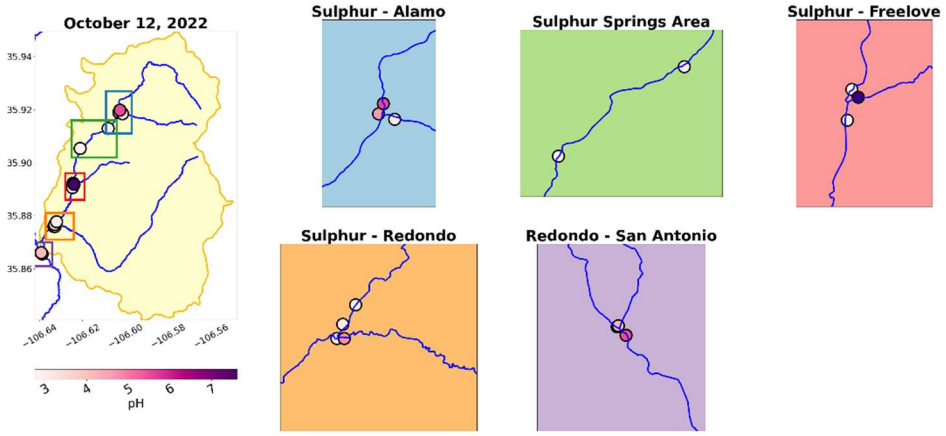
October 12, 2022
35.94
35.92
35.90
35.88
35.86
−106.64
−106.62
−106.60
−106.58
−106.56
3
4
5
6
7
pH
Sulphur - Alamo
Sulphur Springs Area
Sulphur - Freelove
Sulphur - Redondo
Redondo - San Antonio

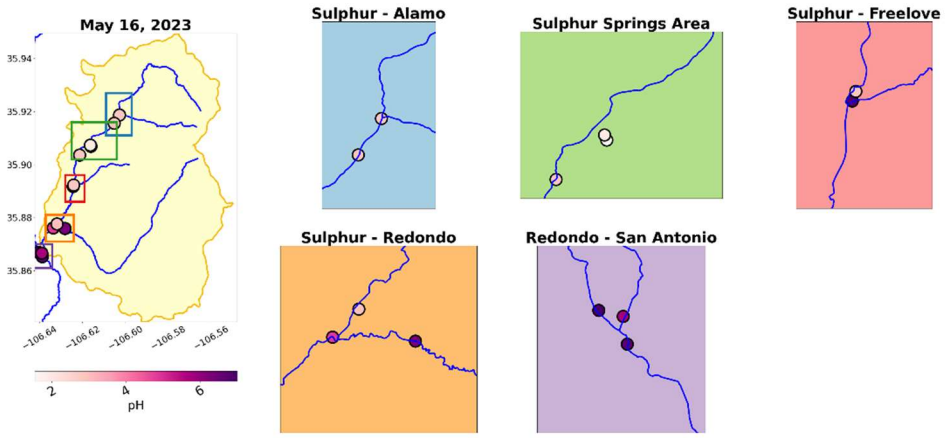
May 16, 2023
35.94
35.92
35.90
35.88
35.86
−106.64
−106.62
−106.60
−106.58
−106.56
2
4
6
pH
Sulphur - Alamo
Sulphur Springs Area
Sulphur - Freelove
Sulphur - Redondo
Redondo - San Antonio